이학박사학위논문

Side Branch Formation in Mammary Glands by ID2 Through the Induction of Differentiation into Luminal Progenitor Cells

ID2 단백질의 유선내강전구세포 분화 유도를 통한 유선 곁가지 생성

2018년 8월

서울대학교 대학원

자연과학대학 생명과학부

성 진 우

ID2 단백질의 유선내강전구세포 분화 유도를 통한 유선 곁가지 생성

지도교수 공 영 윤

이 논문을 이학박사 학위논문으로 제출함
2018년 8월

서울대학교 대학원
자연과학대학 생명과학부
성 진 우

성진우의 이학박사 학위논문을 인준함
2018년 6월

위 원 장 _____ (인)

부위원장 _____ (인)

위 원 _____ (인)

위 원 _____ (인)

위 원 _____ (인)

Side Branch Formation in Mammary Glands by ID2 Through the Induction of Differentiation into Luminal Progenitor Cells

A dissertation submitted in partial
Fulfillment of the requirement for the degree of

DOCTOR OF PHILOSOPHY

To the Faculty of
School of Biological Sciences
at
SEOUL NATIONAL UNIVERSITY
By
Jinwoo Seong

Date Approved:

June, 2018

Committee Chair: _____

Vice Chair: _____

Member: _____

Member: _____

Member: _____

ABSTRACT

Side Branch Formation in Mammary Glands by ID2 Through the Induction of Differentiation into Luminal Progenitor Cells

Jinwoo Seong

School of Biological Sciences

The Graduate School

Seoul National University

Mammary glands develop through primary ductal elongation and side branching to maximize the spatial area. Primary ducts are the initial ducts extending directly from nipple, and have highly proliferative mass of cells in the foremost-end of ducts, named terminal end buds (TEBs). Through bifurcation of TEB, primary ducts gradually fill fat pads. As primary ductal elongation occurs, new branches are budded out laterally from the middle of primary ducts, which is called lateral or side branching. A recent study revealed that primary duct determines direction and speed of elongation through spatial growth inhibition of each other, however, the mechanism through which side

branching occurs and elongates still remains elusive.

It is generally believed that mammary stem cells (MaSCs) differentiate into bipotent progenitor cells that further differentiate into either luminal or myoepithelial lineage cells. However, since there is no specific marker to label MaSC yet, it is very difficult to trace the progeny of MaSC, and the mechanism by which stem and bipotent progenitor cells differentiate into specific lineage cells remains to be determined. Therefore, revealing the differentiation mechanism of stem and bipotent progenitor cells is a crucial step to understand mammary gland development.

Here, I show that inhibitor of DNA-binding 2 (ID2) drives side branch formation through differentiation of $K6^+$ bipotent progenitor cells into $CD61^+$ luminal progenitor cells. *Id2*-null mice had side branching defects, along with developmental blockage of $K6^+$ bipotent progenitor cells into $CD61^+$ luminal progenitor cells. Contrary to *Id2*-null mice, *MMTV-NLS-Id2* transgenic mice showed dramatically increased side branches with active differentiation of $K6^+$ bipotent progenitor cells into $CD61^+$ luminal progenitor cells. Notably, $CD61^+$ luminal progenitor cells were found in budding and side branches, but not in primary ducts and TEBs, indicating that $CD61^+$ luminal progenitor cells are implicated in side branching. Hormone reconstitution studies using ovariectomized *MMTV-NLS-Id2* transgenic mice revealed

that ID2 is a key mediator of progesterone, which drives luminal lineage differentiation and side branching. Taken together, in developing mammary glands, I suggest that ID2 induces differentiation of $K6^+$ bipotent progenitor cells into $CD61^+$ luminal progenitor cells in putative side branching points as a key mediator of progesterone.

Key word: mammary glands, inhibitor of DNA-binding 2 (ID2), CD61, luminal progenitor cells, side branching

Student Number: 2010-23112

CONTENTS

LIST OF FIGURES

BACKGROUND

Development of Mammary Gland

Mammary gland, or milk-producing tissue, is a mammalian specific organ whose product 'milk' is used to breed their offspring. Unlike other organs, fetal mammary gland development is negligible, and the organ is gradually differentiated by hormones after adolescence (Howlin et al., 2006; Robinson, 2007). At embryonic day 11.5 (E11.5), the first mammary placode is observed. From E13.5 and onward, mammary epithelial cells invaginate into mesenchyme cells and form 'mammary buds'. At E15.5, around the mammary buds, fat pad begins to be generated through aggregation of fat pad precursor. Rudimentary ducts are observed at E18.5, and cease ductal elongation until puberty (Fig. 1).

Branching is a typical process in the postnatal mammary gland development. The first sprouting duct, called 'primary duct', of mammary glands has a foremost-proliferative mass of cells, called 'terminal end bud (TEB)', which fills fat pad gradually by bifurcation. New branches are budded out laterally from the middle of the primary ducts by progesterone, an action called lateral or side branching (Atwood et al., 2000; Aupperlee et al., 2013; Brisken, 2013). During pregnancy, additional side branching is observed and milk-producing lubulo-alveolar structure is formed at the end of side branches (Fig. 2).

Figure 1. Schematic view of mammary gland development. Mouse embryo has five pair of mammary placodes, and these placodes develop into mammary buds and rudimentary glands. By E18.5, rudimentary mammary gland remains quiescent until puberty. (Gjorevski and Nelson, 2011)

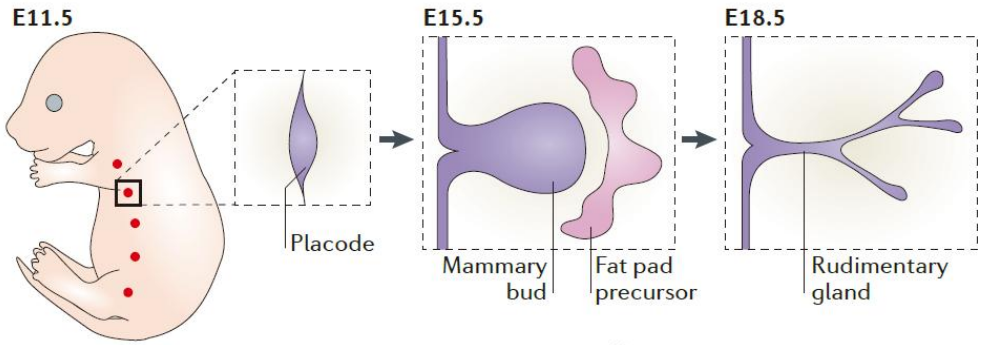
E11.5
Placode
E15.5
Mammary bud
Fat pad precursor
E18.5
Rudimentary gland

Figure 2. Mouse mammary gland development during puberty, pregnancy and lactation. During puberty, primary ductal elongation occurs by bifucatuion of TEBs. New side branches are formed in the middle of primary ducts. Further side branching and lobulo-alveologenesis occurs during pregnancy. (Hennighausen and Robinson, 2005)

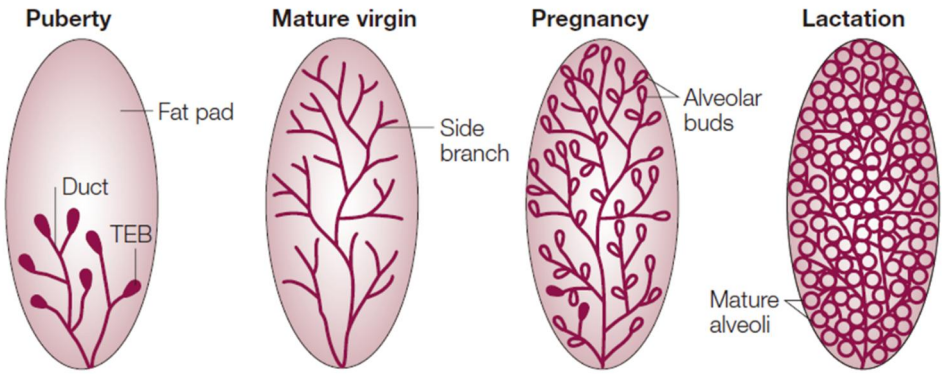
Puberty
Fat pad
Duct
TEB
Mature virgin
Side branch
Pregnancy
Alveolar buds
Lactation
Mature alveoli

Anatomy of Mammary Gland

Mammary epithelial cells (MECs) are composed of two main cell types – luminal and myoepithelial cells. The luminal cells reside in the interior of the duct, and are subdivided into two sub-types according to their function and position – milk producing alveolar cells in the lobulo-alveoli, and ductal cells in ducts which provide passage to milk flow (Visvader and Stingl, 2014). Myoepithelial cells reside in the periphery of the ducts as a thin single layer, surrounding the luminal cells. Myoepithelial cells support ductal structure and help the milk passage by contracting the ducts (Fig. 3) (Brisken and Duss, 2007; Hennighausen and Robinson, 2005; Visvader and Stingl, 2014). Myoepithelial cells are also known as 'basal cells' since myoepithelial cells reside adjacent to the basement membrane. However, the term 'basal cells' includes not only myoepithelial cells but also all cells located near the basement membrane, although it is still not clear which type of cells reside in the basal region.

The foremost region of the elongating primary duct is called the 'terminal end bud (TEB)', as described above (Fig. 2, 3). Since the cells in TEBs actively proliferate, it is believed that TEBs have an abundance of stem/progenitor cells rather than mature cells (Gajewska et al., 2013; Hannezo et al., 2017; Scheele et al., 2017; Woodward et al., 2005). Therefore, the cells which reside in the interior and periphery of TEBs are named as body and cap cells instead of luminal and myoepithelial cells, respectively. Different from ducts which have single-layered

luminal cells, TEBs have multi-layered body cells and undergo apoptosis as ductal elongation progresses (Smalley and Ashworth, 2003).

Figure 3. Mammary epithelial cells in a duct (A) and a TEB (B). The luminal cells reside interior of duct and myoepithelial cells reside in periphery of duct. Basement membrane surrounds mammary epithelial cells. (Visvader, 2009)

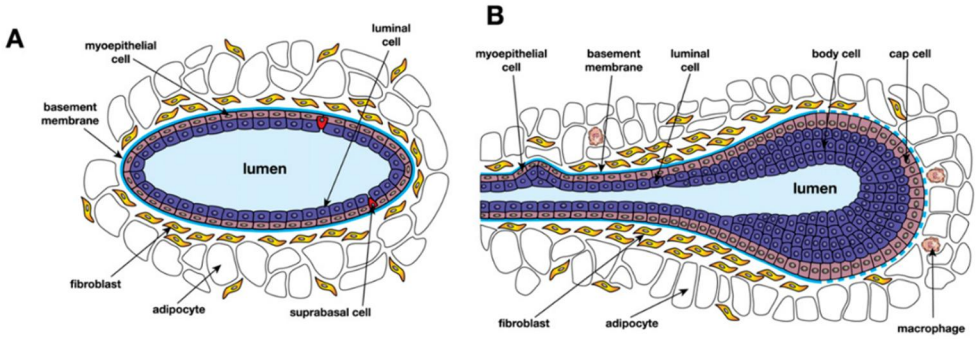
A
myoepithelial cell
luminal cell
basement membrane
lumen
fibroblast
adipocyte
suprabasal cell
B
myoepithelial cell
basement membrane
luminal cell
body cell
cap cell
lumen
fibroblast
adipocyte
macrophage

Hierarchy of Mammary Epithelial Cell

Since there are no proper markers to label mammary stem cells (MaSCs) yet, it is still not clear where the stem cells reside and what lineage they differentiate into. To investigate where the stem cells reside, transplantation experiments have been performed. Since adult stem cells are able to generate whole tissue after transplantation, either luminal or basal cells were transplanted into 'cleared fat pads' (the remained fat pads after removal of all mammary glands in 3-week-old recipient mice. Fig. 4). Transplantation of basal cells was sufficient to form whole mammary glands while transplanted luminal cells formed aberrant ductal trees, indicating that basal cells include multi-potent MaSCs as well as mature myoepithelial cells (Fig. 5) (Prater et al., 2014; Rios et al., 2014; Shackleton et al., 2006; Stingl, 2009; Stingl et al., 2006; Van Keymeulen et al., 2011).

It is generally believed that MaSCs differentiate into bipotent progenitor cells, myoepithelial / luminal progenitor cells, and mature myoepithelial / luminal cells, in progression. K6 was suggested as marker for bipotent progenitor cells because transplanted $K6^+$ cells showed limited ductal outgrowth but differentiated into both luminal and myoepithelial cells (Bu et al., 2011; Grimm et al., 2006; Smith et al., 1990; Sun et al., 2010). However, the mechanism by which $K6^+$ bipotent progenitor cells differentiate into myoepithelial or luminal progenitor cells is still unknown.

So far, there are no markers that allow us to distinguish myoepithelial

progenitor cells from mature myoepithelial cells yet. In case of luminal cells, CD61 (Integrin-β3)$^{+}$ luminal cells were suggested as luminal progenitor cells (Asselin-Labat et al., 2007), and *Cd61*-null mice showed lobulo-alveologenesis defect during pregnancy (Desgrosellier et al., 2014). CD61^{+} luminal progenitor cells further differentiate into mature luminal cells (alveolar and ductal cells) by hormones and factors, such as E74-like factor 5 (ELF5), GATA-3 and Signal transducer and activator of transcription 5 (STAT5) (Asselin-Labat et al., 2007; Chakrabarti et al., 2012; Choi et al., 2009; Cui et al., 2004; Desgrosellier et al., 2014; Kouros-Mehr et al., 2006; Lee et al., 2013; Miyoshi et al., 2001; Oakes et al., 2008).

In order to discriminate luminal cells from myoepithelial cells, immunohistochemistry (IHC) and flow cytometry are generally used. In IHC analysis, luminal cells can be detected through expression of cytokeratin 8, 18, 19 (K8, K18, K19), and myoepithelial cells through cytokeratin 5, 14 (K5, K14) and alpha smooth muscle actin (α-SMA). In flow cytometry analysis, CD29^{mid}CD24^{high} and CD29^{high}CD24^{+} population represent luminal cells and basal/myoepithelial cells, respectively (Shackleton et al., 2006).

Figure 4. Clearing of inguinal fat pad. Since mammary glands of 3-week-old mice cannot elongate to near the lymph node, all mammary ducts are removed through resection from nipple to lymph node. Remained fat pad (cleared fat pad) is used for transplantation experiments. (Smalley and Ashworth, 2003)


Wholemount of 3-week-old fat pad
Wholemount of cleared fat pad
Wholemount of cleared fat pad
8 weeks after transplantation of
primary mammary epithelial cells
Nipple
Line of surgery
for clearing
Lymph node

Figure 5. Transplantation of basal cells or luminal cells into cleared fat pad. The basal transplant shows intact ductal elongation while the luminal transplant has aberrant ductal trees. (Bu et al., 2011)

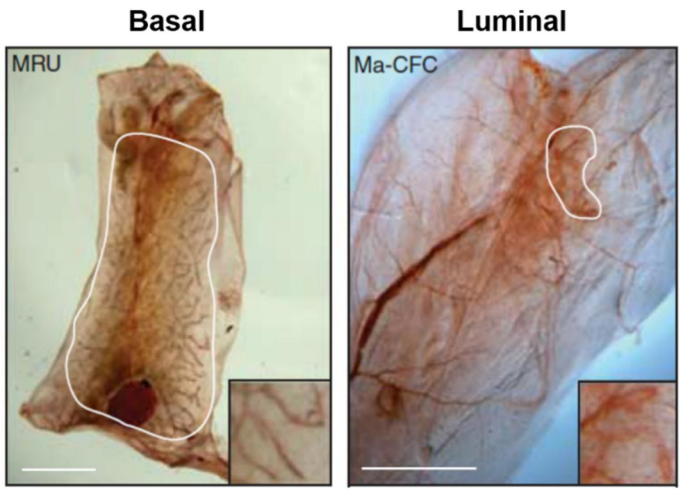
Basal
Luminal
MRU
Ma-CFC

Roles of Ovarian Hormones in Mammary Gland Development

Virgin mammary gland development is strongly influenced by ovarian hormones, such as estrogen and progesterone. Approximately 30-40% of luminal cells have estrogen-alpha receptor (ESR1) and progesterone receptor (PGR), and these cells are called 'sensor cells' (Brisken and Duss, 2007; Rajaram et al., 2015). Sensor cells recognize hormones and induce further signaling.

Estrogen induces proliferation of TEBs and primary ductal elongation (Ciarloni et al., 2007). Through unknown mechanisms, estrogen also induces PGR expression, which is responsible for approximately 80% of total PGR expression (Haslam, 1988a, b). In turn, progesterone induces side branch formation and luminal lineage differentiation (Fig. 6). Through paracrine mediators, such as receptor activator of nuclear factor-κB ligand (RANKL) and WNT4, progesterone induces massive proliferation of progenitor and stem cells in putative side branch points (Beleut et al., 2010; Grimm et al., 2016; Joshi et al., 2010). These results indicate that cooperation of estrogen and progesterone is essential for mammary gland development.

RANKL is a transcriptional target of progesterone and a pivotal mediator of progesterone signaling for mammary gland development. *Rankl*$^{-/-}$ mice showed lobulo-alveologenesis defect like *Pgr*$^{-/-}$ mice (Fata et al., 2000), and *Rankl*-transgenic (*Rankl* Tg) mice showed massive side branching and alveologenesis similar to the progesterone administered mice. Moreover, overexpression of

RANKL rescued side branching defects in *Pgr*-null mice (Beleut et al., 2010; Fernandez-Valdivia et al., 2009; Mukherjee et al., 2010), indicating that progesterone induces side branch formation and luminal lineage differentiation through RANKL.

Figure 6. Whole-mount staining of mouse inguinal mammary glands after progesterone pellet implantation. (A) Control and (B) progesterone pellet-administered mice. Progesterone induces side branch formation. (Atwood et al., 2000)

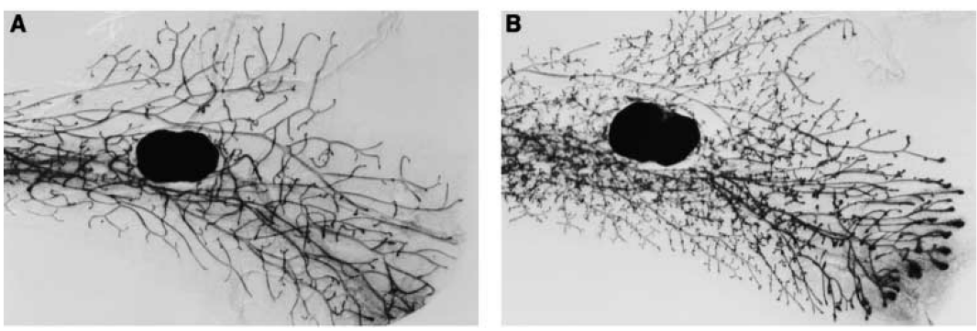
A
B

Menstrual Cycle and Side Branching

In female virgin mice, the concentration of estrogen and progesterone fluctuate in regular intervals rather than always being maintained at constant levels. Depending on the relative concentration of estrogen and progesterone, menstrual cycle (estrus cycle) occurs. For mice, the estrus cycle is composed of four stages: Proestrus, estrus, metestrus, and diestrus. Each stage is easily discriminated from another by the component of vaginal secretion. Mice at diestrus and estrus are characterized by leukocytes and cornified epithelial cells, respectively (Byers et al., 2012).

Diestrus and estrus are the stage at which the levels of progesterone are the highest and lowest in virgin mice, respectively (Joshi et al., 2010). The number of side branches in diestrus females was significantly higher than any other stages, indicating that progesterone is crucial for side branching.

Function of ID proteins in Mammary Gland

There are four different forms of Inhibitor of DNA binding or Inhibitor of differentiation (ID) proteins: ID1, ID2, ID3, and ID4. Because ID proteins belong to the helix-loop-helix (HLH) family, they tend to bind other basic helix-loop-helix (bHLH) proteins (also known as E proteins) to form homo- or heterodimers through their highly conserved HLH domain (Norton et al., 1998). Due to the absence of the basic domain, which binds DNA, ID proteins prevent other bHLH proteins from binding the DNA, acting as negative regulators (Fig. 7). In this way, ID proteins control developmental procedures in many tissues from embryonic period to adult tissue development, by regulating cell growth, death, and differentiation (Benezra, 2001; Lasorella et al., 2014; Niola et al., 2012; Park et al., 2013; Parrinello et al., 2001; Ruzinova and Benezra, 2003; Verykokakis et al., 2013; Zebedee and Hara, 2001).

Although all ID proteins have conserved domains, each ID protein has different roles in different cell types (Coppe et al., 2003; Lasorella et al., 2001). In mammary gland, neither *Id1*- or *Id3*-null mice had a significant phenotype. ID4 is exclusively expressed in basal cells and *Id4*-null mice showed ductal elongation defects (Dong et al., 2011). *Id2*-null mice had perinatal lethality (about 25%) as well as severely weakened immune system (de Candia et al., 2004; Yokota et al., 1999; Yokota et al., 2001). In mammary glands, ID2 is highly expressed during pregnancy and ID2 null mice showed lobulo-alveologenesis defects during

pregnancy with lack of milk production. So far, it has been believed that ID2 is involved in lobulo-alveolar differentiation during pregnancy but has negligible effect in developing mammary gland of young virgin mice (Miyoshi et al., 2002; Mori et al., 2003; Mori et al., 2000).

RANKL, a key mediator of progesterone signaling, induces nuclear retention of ID2 in lactating mammary glands (Kim et al., 2006; Kim et al., 2011). Pregnant *Rankl*$^{-/-}$ mice shows impaired luminal lineage differentiation and lobulo-alveologenesis. However, forced nuclear retention of ID2 rescues all defects of *Rankl*$^{-/-}$ mice, suggesting that ID2 nuclear localization may be a critical step for luminal lineage differentiation by the progesterone-RANKL axis.

Figure 7. Working mechanism of ID proteins. (A) In the absence of ID proteins, bHLH proteins heterodimerized with other bHLH proteins and induce gene transcription. (B) ID proteins sequester bHLH and inhibit binding to other bHLH proteins, resulting in blockage of transcription. (de Candia et al., 2004)

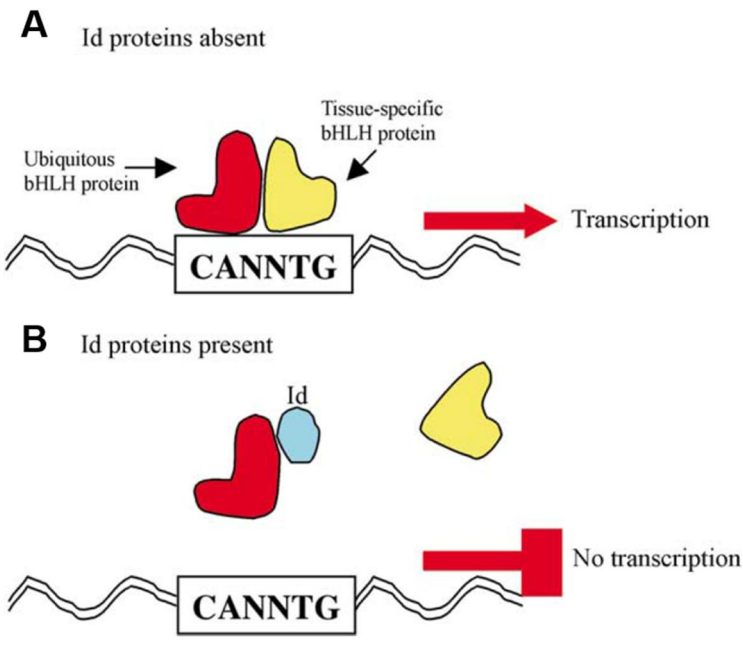
A
Id proteins absent
Tissue-specific
bHLH protein
Ubiquitous
bHLH protein
Transcription
CANNTG
B
Id proteins present
Id
No transcription
CANNTG

Mammary Tumorigenesis

There are six different subtypes of breast cancer, depending on the origin cells of tumor (Normal-like, Luminal A, Luminal B, HER2-enriched, Basal-like, Claudin-low; Fig. 8) (Prat and Perou, 2009). Among the six subtypes of tumor, HER2-enriched tumor is the most prevalent type of tumor and occupies 30~40% of cause of total breast cancer.

NEU (also known as HER2, ERBB2) belongs to the epithelial growth factor receptor (EGFR) family, and constitute activation of NEU signaling results in aberrant cell proliferation and HER2-enriched tumor. Therefore, *MMTV (mouse mammary tumor virus)-active Neu*-transgenic (*Neu* Tg) mouse model is widely used for investigation of breast cancer. Since overexpression of NEU evokes $CD61^+$ luminal progenitor-derived tumors (Lo et al., 2012; Prat and Perou, 2009; Vaillant et al., 2008), *Neu* Tg can be used for investigation of proliferation or differentiation of $CD61^+$ luminal progenitor cells.

Figure 8. Model of the mammary epithelial cell hierarchy linked to tumor subtype. Since basal cells have mammary stem cell, basal cell origin tumors show poor prognosis. Overexpression of NEU results in occurrence of HER2-enriched tumor. (Prat and Perou, 2009)

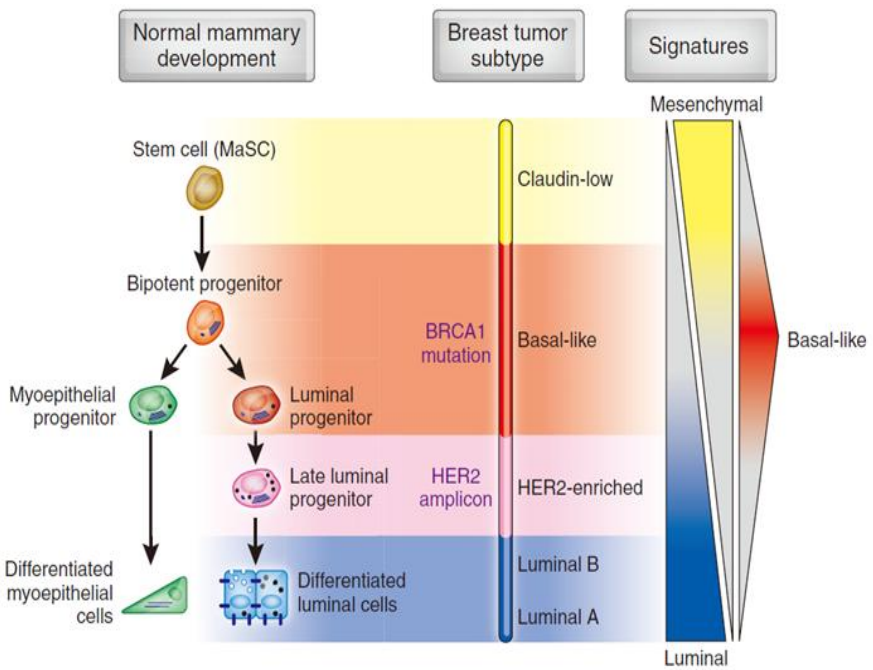
Normal mammary development
Breast tumor subtype
Signatures
Mesenchymal
Stem cell (MaSC)
Claudin-low
Bipotent progenitor
BRCA1 mutation
Basal-like
Basal-like
Myoepithelial progenitor
Luminal progenitor
Late luminal progenitor
HER2 amplicon
HER2-enriched
Differentiated myoepithelial cells
Differentiated luminal cells
Luminal B
Luminal A
Luminal

INTRODUCTION

From the adolescent stage, mammary glands gradually differentiate into mature glands through the functions of ovarian hormones, such as estrogen and progesterone (Howlin et al., 2006; Robinson, 2007). Primary ducts of mammary glands have a proliferative mass of cells, called terminal end buds (TEBs), which progressively fill fat pads through bifurcation. Along with primary ductal elongation, new branches bud out laterally from the primary ducts; this process is called lateral or side branching. Since side branching has to occur to enable adequate production of milk during lactation, many studies have evaluated how ovarian hormones affect side branching. Progesterone receptor (PGR) null ($Pgr^{-/-}$) mice exhibit fewer side branches compared to controls, and transplanted mammary epithelial cells (MECs) from $Pgr^{-/-}$ ducts into cleared fat pads show defects in side branching (Brisken et al., 2000; Lydon et al., 1995; Soyal et al., 2002). In contrast, progesterone pellet treatment in peripubertal mice enhances side branching (Atwood et al., 2000), indicating that progesterone is a key regulator of side branching. To date, many studies have revealed factors that control the formation of side branches, including progesterone and its downstream mediator receptor activator of nuclear factor-κB ligand (RANKL) (Beleut et al., 2010; Brisken et al., 2000; Fernandez-Valdivia et al., 2009; Mukherjee et al., 2010; Rajaram et al., 2015). However, the mechanisms through which side branches are formed still require further investigation.

Mammary stem cells (MaSCs) differentiate into bipotent progenitor cells (BPs) that further differentiate into either luminal or myoepithelial progenitor cells (Brisken and Duss, 2007; Hennighausen and Robinson, 2005; Visvader and Stingl, 2014). CD61 (integrin-β3) has been suggested as a marker for luminal progenitor cells (LPs) (Asselin-Labat et al., 2007), which differentiate into mature luminal cells, namely ductal and alveolar cells. E74-like factor 5 (ELF5) and GATA-3 induce terminal luminal differentiation of $CD61^+$ LPs into alveolar cells (Chakrabarti et al., 2012; Choi et al., 2009; Cui et al., 2004; Kouros-Mehr et al., 2006; Lee et al., 2013; Oakes et al., 2008), and pregnant *Cd61*-null mice show defects in lobulo-alveologenesis (Desgrosellier et al., 2014), suggesting that CD61 is essential for luminal lineage differentiation. Although many researchers have demonstrated the importance of $CD61^+$ LPs in luminal lineage differentiation, the factors inducing the differentiation of stem/bipotent progenitor cells into $CD61^+$ LPs yet remain to be determined.

There are four different forms of Inhibitor of DNA-binding (ID) proteins: ID1, ID2, ID3, and ID4. Although they all have a helix-loop-helix (HLH) domain (Norton et al., 1998), their respective functions in mammary glands differ from one another. *Id1* or *Id3* single null mice show normal mammary gland development (de Candia et al., 2004; Lyden et al., 1999), whereas ID4 is a key regulator of MaSC self-renewal in basal cells (Best et al., 2014; Dong et al., 2011; Junankar et al., 2015). ID2 is highly expressed during pregnancy, and $Id2^{-/-}$ mice have defects in

lobulo-alveologenesis and induction of milk protein genes at pregnancy (de Candia et al., 2004; Miyoshi et al., 2002; Mori et al., 2003; Mori et al., 2000; Parrinello et al., 2001; Yokota et al., 1999; Yokota et al., 2001). Based on phenocopy between *Id2*$^{-/-}$ and *Rankl*$^{-/-}$ mice at pregnancy, our laboratory previously reported that RANKL drives nuclear retention of ID2 in MECs, and forced nuclear retention of ID2 rescues luminal differentiation defects in *Rankl*$^{-/-}$ mice (Kim et al., 2006; Kim et al., 2011). Since RANKL is a key mediator of progesterone in side branching and the expansion of luminal cells (Beleut et al., 2010; Fata et al., 2000; Fernandez-Valdivia et al., 2009; Mukherjee et al., 2010; Obr et al., 2013), ID2 may be a putative downstream mediator of the progesterone/RANK signaling axis for side branching and luminal lineage commitment.

In this study, I found that ID2 induces side branch formation by inducing differentiation of K6^{+} BPs into CD61^{+} LPs in virgin mammary glands. *Id2*$^{-/-}$ mice showed accumulation of K6^{+} BPs and dramatic reduction of CD61^{+} LPs with few side branches, while *MMTV-hemagglutinin (HA)-nuclear localized sequence (NLS)-tagged-Id2 transgenic* (*NLS-Id2* Tg) mice showed prolific induction of side branching. Importantly, most CD61^{+} LPs were found in budding and side branches, but were rarely detected in primary ducts and TEBs, indicating that differentiation of CD61^{+} LPs is involved in side branch formation rather than primary ductal elongation. Hormone reconstitution studies using ovariectomized (Ovx) *NLS-Id2* Tg mouse model revealed that nuclear ID2 is a downstream mediator of progesterone for side branching and luminal lineage differentiation. My study will

provide critical insights into how side branches are formed in developing virgin mammary glands.

RESULTS

Side branching defects in *Id2*$^{-/-}$ virgin mice

Previous studies reported that *Id2*$^{-/-}$ mice had normal ductal trees in nulliparous females, but showed defects in lobulo-alveologenesis during pregnancy (Miyoshi et al., 2002; Mori et al., 2000). Since lobulo-alveolar cells are differentiated from LPs (Brisken and Duss, 2007; Hennighausen and Robinson, 2005; Visvader and Stingl, 2014), I hypothesized that the lobulo-alveologenesis defects of *Id2*$^{-/-}$ mice at pregnancy might be secondary defects caused by impaired luminal lineage differentiation in virgins. Hence, I carefully re-examined the development and morphogenesis of virgin *Id2*$^{-/-}$ mammary glands. Consistent with previous reports, whole-mount carmine-alum (C-A) staining of mammary glands from 4- and 8-week-old virgin *Id2*$^{-/-}$ mice showed intact TEBs and normal fat pad coverage of primary and secondary ducts (ducts formed by bifurcation of TEBs), similar to wild-type (WT) mice (Fig. 9A). Interestingly, the number of tertiary branches (terminal side branches) were dramatically reduced in virgin *Id2*$^{-/-}$ mice (0.11-fold) (Fig. 9B). I also quantified nascent side branches (the points at which side branches will bud out), which are identified through deeply colored spots in C-A staining (Sternlicht et al., 2006). Hematoxylin and Eosin (H&E) and C-A staining of mammary glands showed that *Id2*$^{-/-}$ mammary glands exhibited few deeply colored nascent side branches (hereafter, nascent branches) and budding side branches (hereafter, budding branches), but showed an intact terminal end bud structure (Fig.

9C). The side branching defects were evident, even at 20 weeks of age (Fig. 10 A–C), indicating that side branching defects in *Id2*$^{-/-}$ mice are not due to delayed development of mammary glands.

To investigate whether the side branching defects in *Id2*$^{-/-}$ mice are cell intrinsic or extrinsic, e.g., hormones or niches, I performed transplantation experiments. MECs from 8-week-old WT and *Id2*$^{-/-}$ mice were transplanted into the cleared fat pads of 3-week-old WT mice (Fig. 11A). Eight weeks after transplantation, MECs from both genotypes repopulated well in the cleared fat pads. However, tertiary and nascent/budding branches were dramatically decreased in *Id2*$^{-/-}$ donor transplants compared with those of controls (Fig. 12A, B). Taken together, my results showed that ID2 is required for side branching of mammary glands in a cell-intrinsic manner.

Figure 9. Side branching defects in *Id2*$^{-/-}$ virgin mice with intact TEBs. (A, B) Carmine-Alum (C-A)-stained mammary glands (A) and quantification of branches (B) in 8-week-old WT and *Id2*$^{-/-}$ mice. *Id2*$^{-/-}$ mice showed intact TEBs and fat pad coverage of primary ducts. However, side and nascent/budding branches were dramatically decreased in *Id2*$^{-/-}$ mice. All mice were sacrificed at diestrus. Proximal (P), near the nipple; medial (M), near the lymph node; distal (D), outermost region. The circle indicates the nipple. Arrow, side branches; arrowhead, nascent/budding side branches. 1', 2', 3', and N/B represent the primary duct, secondary branch, tertiary branch (terminal side branch), and nascent/budding side branch, respectively. Scale bar, 1 cm; in the enlargements, 1 mm. N=3, each. Data are means ± s.e.m.; Student's t-tests. *p<0.05; **p<0.01; ***p<0.001. **(C)** H&E-stained mammary glands from 8-week-old WT and *Id2*$^{-/-}$ mice. *Id2*$^{-/-}$ mice showed intact end buds. Arrowhead, nascent/budding side branches. Scale bar, 100 μm.

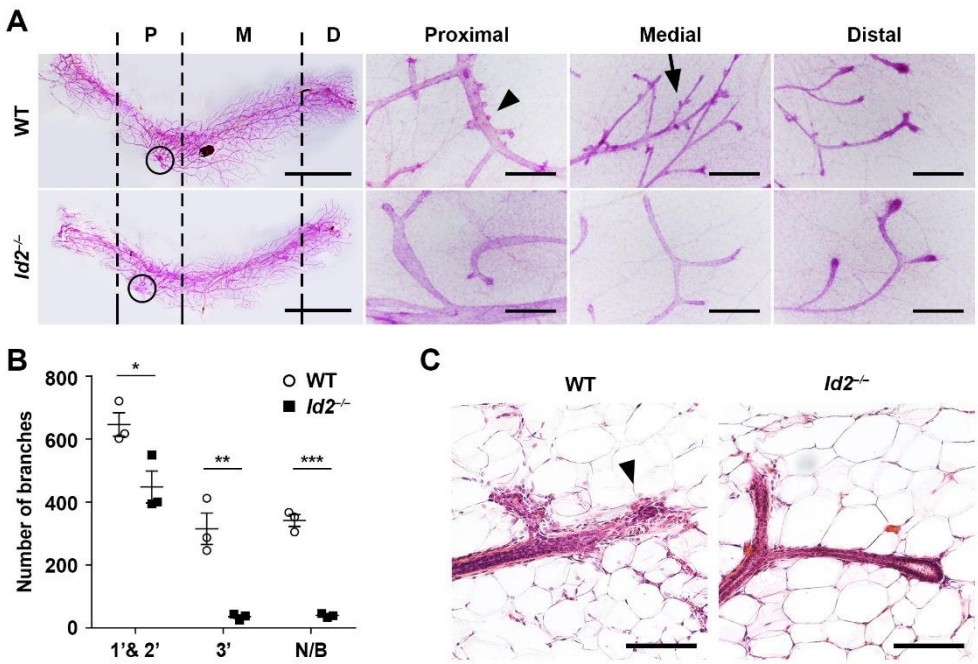
A
P
M
D
Proximal
Medial
Distal
WT
Id2−/−
B
Number of branches
800
600
400
200
0
WT
Id2−/−
*
**
***
1'& 2'
3'
N/B
C
WT
Id2−/−

Figure 10. Non-temporary side branching defects in *Id2*$^{-/-}$ mice. (A–C) C-A-stained inguinal mammary glands (A) and quantification of the number of branches (B, C) in 20-week-old WT and *Id2*$^{-/-}$ mice. Even 20-week-old *Id2*$^{-/-}$ mice had only a few tertiary side and nascent/budding side branches. 3', tertiary branch (terminal side branch); N/B, nascent/budding-side branch. Scale bar, 1 cm; in the enlargements, 0.5 mm. N=3, each. Data are means ± s.e.m.; Student's t-tests. $^{**}p<0.01$.

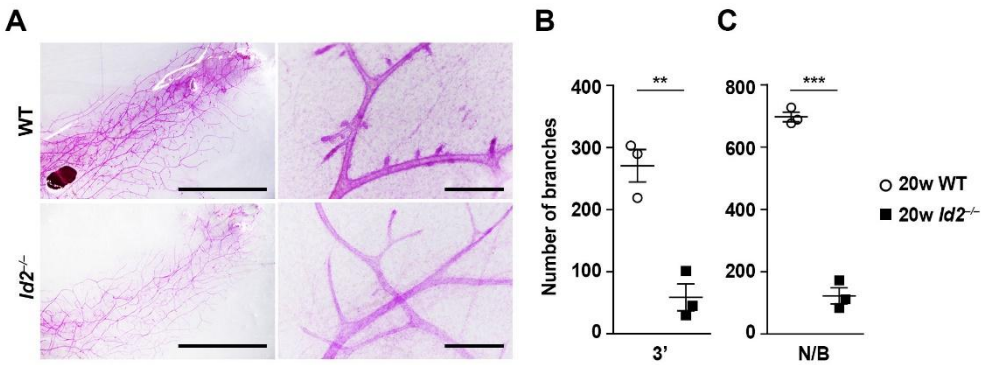
A
WT
Id2-/-
B
Number of branches
400
300
200
100
0
**
3'
C
800
600
400
200
0
***
N/B
20w WT
20w Id2-/-

Figure 11. Schematic view of transplantation. (A) Minced inguinal fat pads of 8-week-old WT and *Id2*$^{-/-}$ mice were transplanted into cleared fat pads of 3-week-old WT recipient mice. After 8–10 weeks, ductal outgrowth was analyzed with C-A staining.

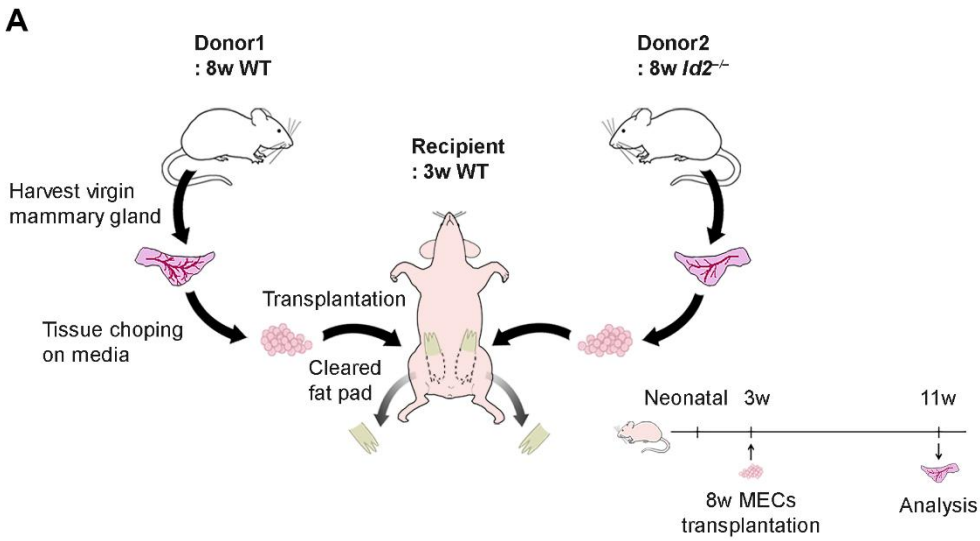
A
Donor1
: 8w WT
Donor2
: 8w Id2−/−
Recipient
: 3w WT
Harvest virgin
mammary gland
Tissue choping
on media
Transplantation
Cleared
fat pad
Neonatal
3w
11w
8w MECs
transplantation
Analysis

Figure 12. Cell autonomous side branching defects in *Id2*$^{-/-}$ virgin mice. (A, B) C-A-stained mammary glands (A) and quantification of branches (B) from transplanted WT and *Id2*$^{-/-}$ MECs. I used 8- and 3-week-old mice as donors and recipients, respectively. The number of tertiary side branches in *Id2*$^{-/-}$ transplants was dramatically decreased compared to that of WT transplants, indicating that ID2 is required for side branching in a cell-intrinsic manner. Circle, transplantation point in cleared fat pads. Arrow, side branches; arrowhead, nascent/budding side branches. Scale bar, 1 cm; in the enlargements, 0.5 mm. N=3, each. Data are means ± s.e.m.; Student's t-tests. *p<0.05; **p<0.01.

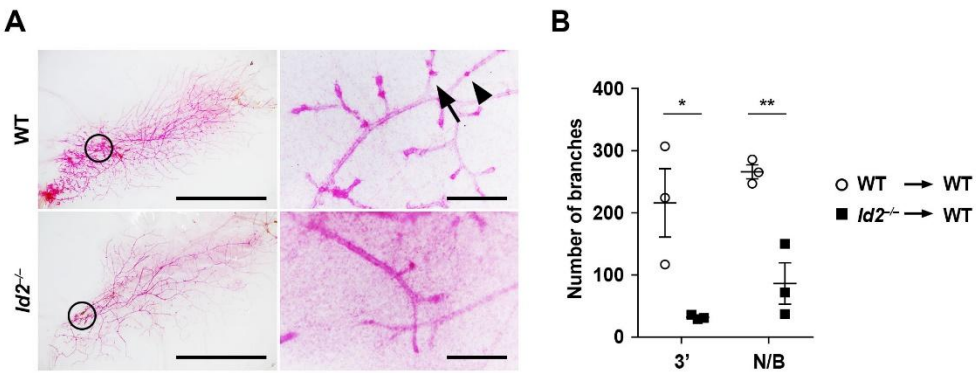
A
WT
Id2-/-
B
Number of branches
400
300
200
100
0
*
**
3'
N/B
WT → WT
Id2-/- → WT

Impaired differentiation into luminal progenitor cells in *Id2*$^{-/-}$ mice

To identify the detailed phenotypes of *Id2*$^{-/-}$ virgin mice, I examined ID2 expression patterns and the cellular composition of *Id2*$^{-/-}$ mammary glands. ID2 was dominantly detected in luminal cells (96.80% ± 2.19%) but barely in basal/myoepithelial cells (2.03% ± 1.19%) (Fig. 13A). Quantitative real-time reverse transcription polymerase chain reaction (qRT-PCR) analysis using freshly isolated MECs showed that the expression levels of luminal markers, i.e., *Cytokeratin 8* (*K8*), *Cytokeratin 18* (*K18*), and *Cytokeratin 19* (*K19*), were significantly decreased in *Id2*$^{-/-}$ MECs compared with those of controls, whereas the expression levels of basal/myoepithelial markers, i.e., *Smooth muscle actin* (*Sma*) and *Cytokeratin 14* (*K14*), were comparable (Fig. 14A, B). A recent study revealed that luminal cells are comprised of K8^{high} and K8^{low} cells (Davis et al., 2016). To examine whether *Id2*$^{-/-}$ mice have reduced luminal population or have just few K8^{high} cells with intact number of luminal cells, I performed immunohistochemistry (IHC) for E-cadherin (E-cad, luminal epithelial cell marker), K8, and K14. Quantification data for IHC and immunoblotting data showed that *Id2*$^{-/-}$ mice have decreased number of both E-cad^{+} luminal cells (0.79-fold) and K8^{high} cells (0.54-fold) (Fig. 15A, B), indicating that deletion of ID2 results in the reduction of whole luminal cells including K8^{high} cells. Constantly, immunoblotting showed decreased expression of E-cad and K8 but not SMA in *Id2*$^{-/-}$ MECs (Fig. 15C), suggesting that ID2 plays important roles in luminal lineage cells.

Id2$^{-/-}$ mice showed side branching defects but had normal TEBs and primary ducts, suggesting that primary ducts of *Id2*$^{-/-}$ mice may have normal cell composition similar to WT mice with reduced number of luminal cells in putative side branch points. Since most of side branches are found in proximal region rather than distal region (Sale et al., 2013), I divided inguinal mammary glands of *Id2*$^{-/-}$ mice into proximal and distal regions, and performed IHC for K8 and SMA. I found that lots of *Id2*$^{-/-}$ ducts in distal region showed intact cell composition or mild reduction of K8^{+} cells, but many *Id2*$^{-/-}$ ducts in proximal region showed severe reduction of K8^{+} cells (Fig. 15A). These results suggest that side branching defects in *Id2*$^{-/-}$ mice may be caused by impaired luminal lineage differentiation.

To further investigate which luminal cells are affected in *Id2*$^{-/-}$ mice, I performed flow cytometry analysis. In *Id2*$^{-/-}$ mice, CD29^{mid}CD24^{high} luminal cells (Shackleton et al., 2006) were significantly reduced compared with those of controls, whereas the population of CD29^{high}CD24^{+} basal/myoepithelial cells was increased, which could be explained by decreased luminal cells. Among CD29^{mid}CD24^{high} luminal cells, interestingly, CD61^{+} LPs (Asselin-Labat et al., 2007) were markedly decreased in *Id2*$^{-/-}$ mice compared with those of controls (0.21-fold) (Fig. 16A, B). qRT-PCR and immunoblotting analysis also showed decreased CD61 expression in *Id2*$^{-/-}$ MECs compared with those in controls (Fig. 15C and 16C). Taken together, my data suggested that ID2 may be required for luminal lineage differentiation and generation of CD61^{+} LPs.

Figure 13. ID2 expression in virgin mice. (A) Immunohistochemistry (IHC) analysis of ID2, K8, and SMA in 8-week-old virgin mammary glands. ID2 was detected exclusively in luminal cells. K8 and SMA represent luminal and basal/myoepithelial markers, respectively. Arrow, $ID2^{+}K8^{+}$ luminal cell; arrowhead, $ID2^{-}SMA^{+}$ myoepithelial cells. Scale bar, 50 μm; in the enlargements, 10 μm.

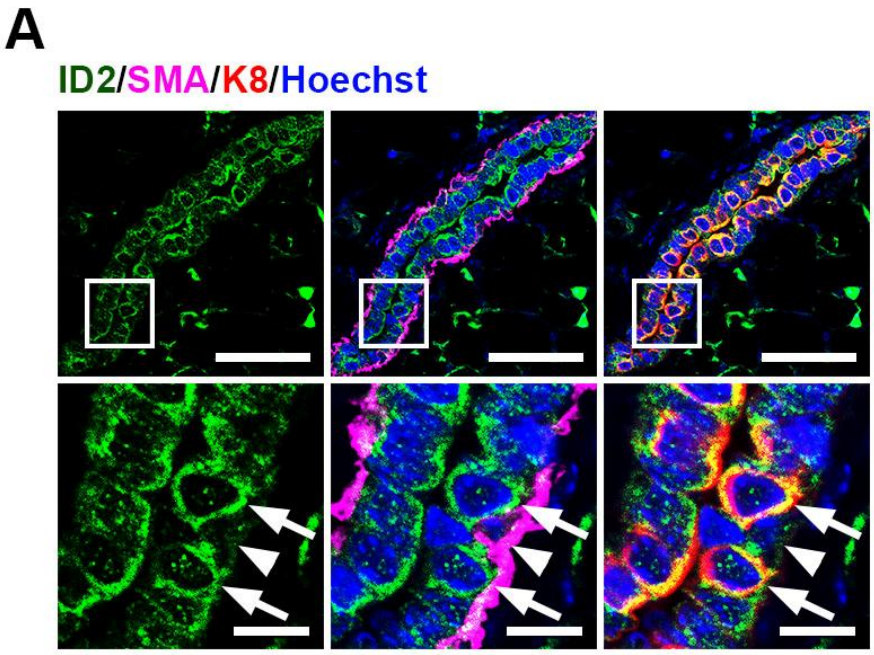
A
ID2/SMA/K8/Hoechst

Figure 14. Reduction of luminal markers in *Id2*$^{-/-}$ mice. (A) mRNA expression of luminal (*K8*, *K18*, and *K19*)- and **(B)**basal/myoepithelial (*Sma* and *K14*) cell markers in WT and *Id2*$^{-/-}$ MECs. All gene expression levels were normalized with *Uxt* (see also Material and Methods). WT (n=7), *Id2*$^{-/-}$ (n=8). Data are means ± s.e.m.; Student's t tests. ***p<0.001

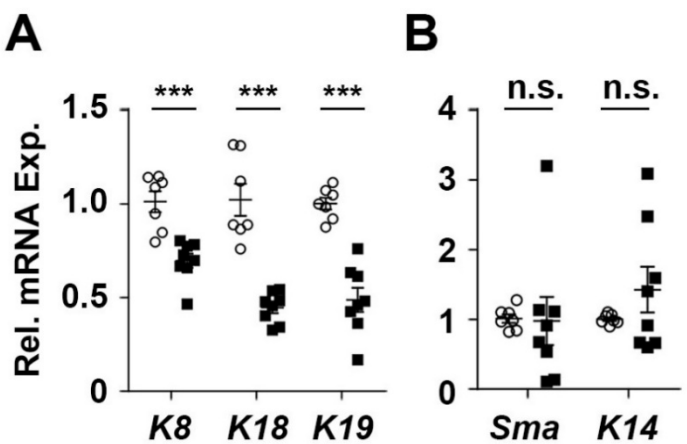
A
B
Rel. mRNA Exp.
1.5
1.0
0.5
0
***
***
***
K8
K18
K19
4
3
2
1
0
n.s.
n.s.
Sma
K14

Figure 15. Decreased number of luminal lineage cells in *Id2*$^{-/-}$ mice. (A, B) IHC staining for K8, E-cad, K14 (A) and quantification of E-cad^{+} and K8^{+} luminal cells in MECs (B) from 8-week-old WT and *Id2*$^{-/-}$ mammary glands. *Id2*$^{-/-}$ mice showed significantly reduced K8^{+} and E-cad^{+} luminal cells with intact K14^{+} cells. Lu, E-cad^{+} luminal cells; K8+, K8^{+} luminal cells. MECs, sum of K14^{+} and E-cad^{+} cells. Scale bar, 30 μm. WT (n=4), *Id2*$^{-/-}$ (n=6). For statistics, I extracted three slides from each mouse. Data are means ± s.e.m.; Student's t tests. ***p<0.001. **(C)** Immunoblotting analysis of isolated WT and *Id2*$^{-/-}$ MECs. β-TUB, β-tubulin.

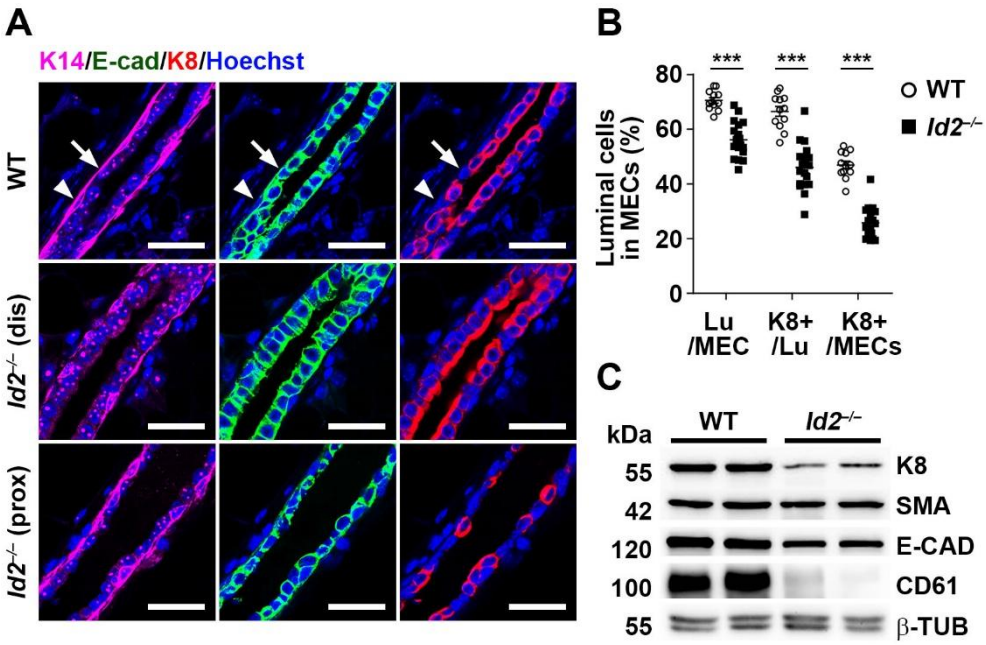
A
K14/E-cad/K8/Hoechst
WT
Id2−/− (dis)
Id2−/− (prox)
B
***
***
***
Luminal cells in MECs (%)
80
60
40
20
0
WT
Id2−/−
Lu /MEC
K8+ /Lu
K8+ /MECs
C
kDa
WT
Id2−/−
55
K8
42
SMA
120
E-CAD
100
CD61
55
β-TUB

Figure 16. Severe reduction of CD61^{+} LPs in *Id2*$^{-/-}$ mice. (A) Flow cytometric analysis of CD29^{mid}CD24^{high} luminal, CD29^{high}CD24^{+} basal/myoepithelial, and CD29^{mid}CD24^{high} CD61^{+} luminal progenitor populations. The CD29-CD61 plot was gated from the CD29^{mid}CD24^{high} luminal population. Luminal cells, particularly CD61^{+} luminal progenitor cells, were dramatically decreased in *Id2*$^{-/-}$ mice. **(B)** Proportion of the luminal population in whole MECs and luminal progenitor population in the luminal population based on flow cytometry data. WT (n=5), *Id2*$^{-/-}$ (n=5). L, luminal; B, basal/myoepithelial cells; LP, luminal progenitor cells. Data are means ± s.e.m.; Student's t tests. ***p<0.001. **(C)** *Cd61* mRNA expression in WT and *Id2*$^{-/-}$ MECs. WT (n=7), *Id2*$^{-/-}$ (n=8). Data are means ± s.e.m.; Student's t tests. ***p<0.001.

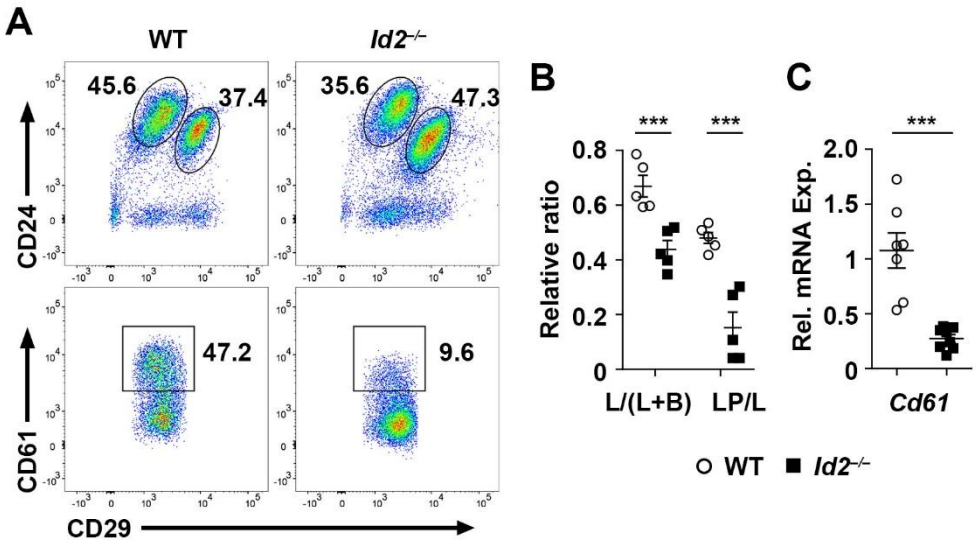
A
WT
Id2−/−
45.6
37.4
35.6
47.3
CD24
47.2
9.6
CD61
CD29
B
***
***
Relative ratio
0.8
0.6
0.4
0.2
0
L/(L+B)
LP/L
C
***
Rel. mRNA Exp.
2.0
1.5
1
0.5
0
Cd61
WT
Id2−/−

Budding and side branch-specific CD61 expression

Based on side branching defects and decreased $CD61^+$ LPs in *Id2*$^{-/-}$ mice, I investigated whether $CD61^+$ LPs are involved in side branching**.** Using traditional methods for mammary tissue preparation, it was difficult to discriminate the side branches from a tilted cut of primary ducts in the cross-section of mammary tissues. To overcome this limitation, I developed a flattened tissue preparation method by dehydrating mammary tissues (see also Material and Methods). Through the improved tissue preparation method, side and budding branches were apparently distinguishable and morphologically distinct from one another. In IHC analysis, surprisingly, CD61 was highly expressed in budding and side branches, but rarely expressed in primary ducts (Fig. 17A).

To prove that $CD61^+$ LPs reside in side branches, I performed 3D mammary tissue imaging with CUBIC (Clear, Unobstructed Brain Imaging Cocktails and computational analysis) method (Lloyd-Lewis et al., 2016; Susaki et al., 2014). My 3D imaging data clearly showed that CD61 was dominantly expressed in laterally budding branches rather than primary ducts, while K8 was ubiquitously expressed in luminal cells, regardless of in primary ducts or side branches (Fig. 18A, B and supplementary movie1, 2). Co-staining of CD61 with K8 showed that most $CD61^+$ cells were negative for K8, although some $CD61^+$ cells were $K8^+$ (Fig. 19A). Since $K8^{high}$ cells are regarded as mature luminal cells with Pgr expression (sensor cells) (Brisken, 2013; Brisken and Duss, 2007; Davis

et al., 2016), CD61 and K8-double positive cells may be differentiating cells from $CD61^+$ LPs into mature $K8^+$ luminal cells or luminal lineage-determined progenitor cells.

TEBs have a characteristic structure with cap cells and multilayered body cells, in which stem/progenitor cells proliferate actively and differentiate into myoepithelial and luminal lineage cells (Gajewska et al., 2013; Scheele et al., 2017; Woodward et al., 2005). Since $CD61^+$ cells have progenitor character, they might reside in TEBs as well as side branches. To examine whether $CD61^+$ LPs also reside in TEBs, I performed IHC on BrdU-incorporated tissues. Unexpectedly, $CD61^+$ cells were barely detected in TEBs (Fig. 20A–C). Collectively, these findings indicate that $CD61^+$ LPs reside in side branches but not in TEBs, suggesting that differentiation of $CD61^+$ LPs is crucial for the formation of side branches but not for primary elongation.

Figure 17. IHC staining for CD61 of flattened mammary gland tissues from 8-week-old WT mice. (A) side and budding branches were apparently distinguishable from primary ducts. CD61 was dominantly expressed in side branches. Scale bar, 200 μm; in the enlargements, 40 μm.

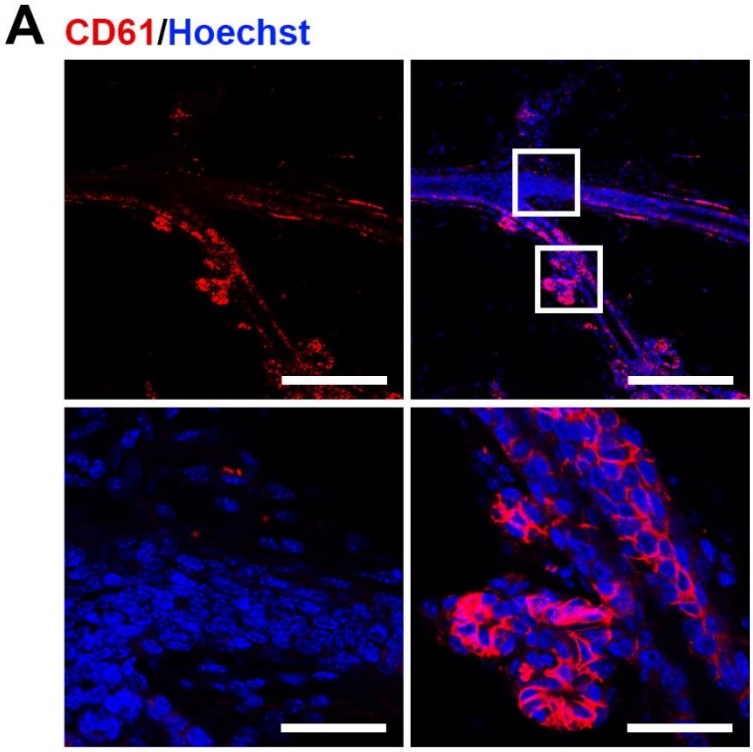
A
CD61/Hoechst

Figure 18. CD61 expression specifically in budding and side branches. (A) low magnification and **(B)** high-magnification of CUBIC tissue clearing and 3D imaging of 8-week-old WT mammary glands. The images were reconstituted with 125 Z-stacks (1 μm-interval). CD61 was dominantly detected in side- and budding branches but barely in primary ducts. Arrowhead, non-specific signals based on rotated view (supplementary movie 1, 2). Scale bar, 200 μm (A); 50 μm (B)

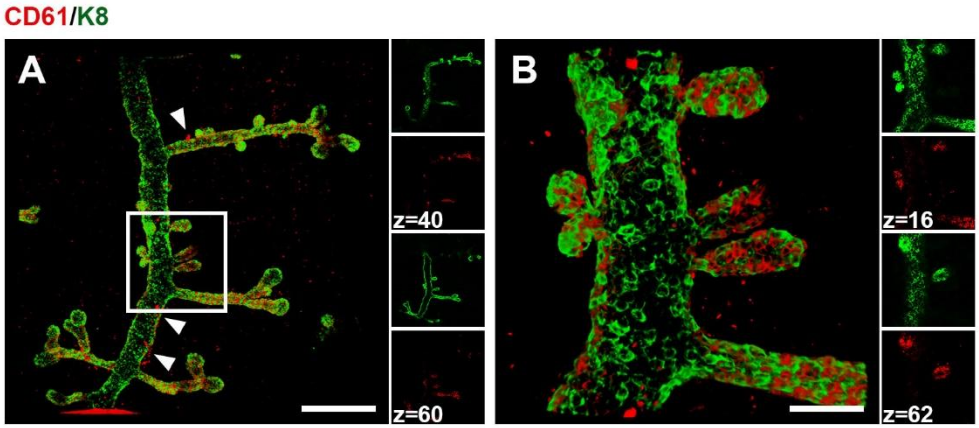
CD61/K8
A
z=40
z=60
B
z=16
z=62

Figure 19. Cell composition of luminal cells in budding and side branches. (A) CD61 single positive cells were dominantly observed in side branches. For statistics, I observed fourteen budding and side branches from three different mice. CD61, $CD61^{+}K8^{-}$ cells; K8, $CD61^{-}K8^{+}$ cells; DP, CD61 and K8 double-positive cells. Data are means ± s.e.m.

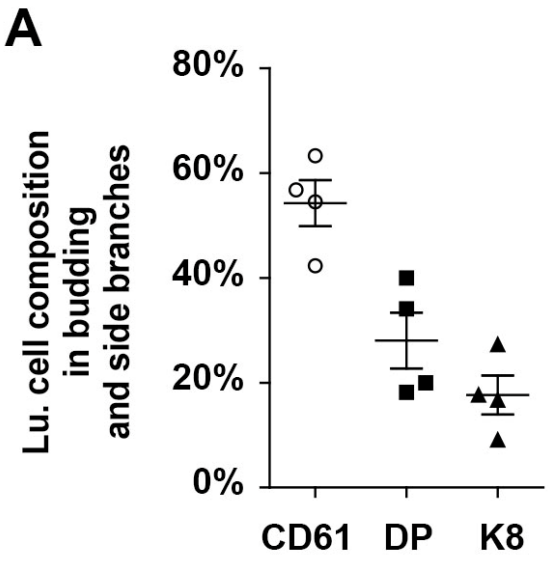
A
Lu. cell composition in budding and side branches
80%
60%
40%
20%
0%
CD61
DP
K8

Figure 20. Lack of CD61$^+$ LPs in TEBs. (A–C) IHC staining for CD61, K8 and BrdU. Terminal end buds were highly proliferative (B) and composed of multilayered body cells (A). CD61 was barely detected in TEBs, whereas numerous CD61$^+$ cells with few BrdU$^+$ cells were detected in side branches (C). Only 1.91% ± 1.41% (Mean ± s.e.m.) of CD61$^+$ cells are BrdU-positive. Scale bar, 50 μm.

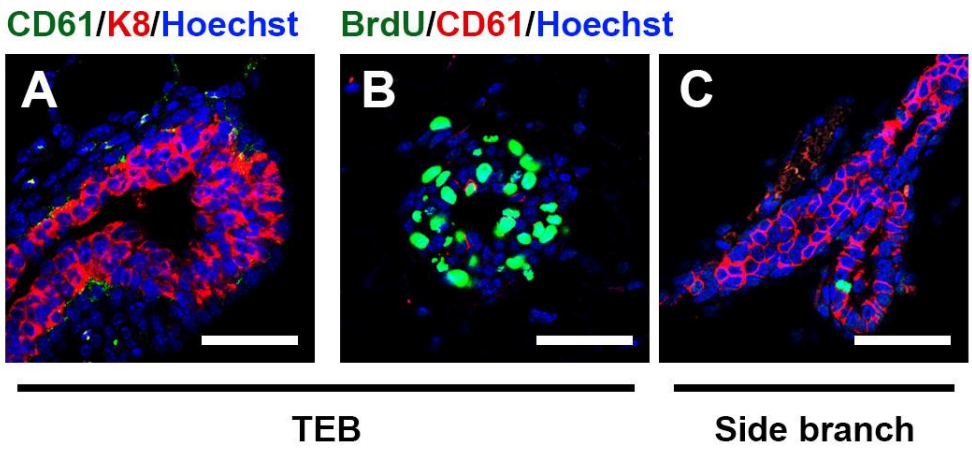
CD61/K8/Hoechst
BrdU/CD61/Hoechst
A
B
C
TEB
Side branch

Accumulation of aberrant K6$^+$ BPs in *Id2*$^{-/-}$ mice

Since CD61$^+$ LPs have been suggested as progenitor cells (Asselin-Labat et al., 2007), decreased CD61$^+$ LPs in *Id2*$^{-/-}$ mice could be due to impaired proliferation of CD61$^+$ LPs. To address this possibility, I performed BrdU incorporation assay. In contrast to my expectation, most CD61$^+$ cells in the side branches were BrdU-negative (Fig. 20C) even in WT mice, suggesting that the reduction of CD61$^+$ LPs in *Id2*$^{-/-}$ mice is not caused by their proliferation defects. To further investigate whether decreased CD61$^+$ LPs in *Id2*$^{-/-}$ mice are caused by developmental blockage of primitive stem/progenitor cells into CD61$^+$ LPs, I examined the expression of K6, a putative marker for BPs (Bu et al., 2011; Grimm et al., 2006; Smith et al., 1990; Sun et al., 2010). K6$^+$ cells were observed in few ducts of 8-week-old WT mice (Fig. 21A, C). Intriguingly, a considerable number of *Id2*$^{-/-}$ ducts showed markedly increased number of K6$^+$ cells with dramatically reduced K8$^+$ mature luminal cells (Fig. 21B, C). Consistent with these findings, qRT-PCR and immunoblotting analyses also showed increased K6 expression in *Id2*$^{-/-}$ mice compared with those in controls (Fig. 22A, B).

To investigate the developmental blockage of K6$^+$ BPs into CD61$^+$ LPs in *Id2*$^{-/-}$ mice, I performed flow cytometry analysis using CD49b (integrin-α2), a promising luminal progenitor marker (Shehata et al., 2012), along with CD61, and revealed that most CD61$^+$ cells were CD49b$^+$ (98.44% ± 0.44%), whereas about 30.40% ± 2.29% CD49b$^+$ cells were CD61$^-$. These data suggest that there are two

distinct subsets of LPs, namely $CD61^{+}CD49b^{+}$ and $CD61^{-}CD49b^{+}$ LPs, in the $CD29^{mid}CD24^{high}$ luminal cell population. $CD61^{+}CD49b^{+}$ LPs were dramatically decreased in *Id2*$^{-/-}$ mice compared with those of controls, whereas $CD61^{-}CD49b^{-}$ population had increased (Fig. 23A), which might be due to increased $K6^{+}$ BPs in *Id2*$^{-/-}$ mice. To address this issue, I sorted out $CD61^{-}CD49b^{-}$ cells and $CD61^{+}CD49b^{+}$ cells from $CD29^{mid}CD24^{high}$ luminal cells and immunostained them with anti-K6 antibody. As expected, $K6^{+}$ BPs were indeed enriched in the $CD61^{-}$ $CD49b^{-}$ population (Fig. 24A, B), and qRT-PCR data also showed increased *K6* expression in the $CD61^{-}CD49b^{-}$ population (Fig. 24C). Consistent with immunohistochemical analysis, the number of $K6^{+}$ cells were greatly increased in $CD61^{-}CD49b^{-}$ population from 6-week-old *Id2*$^{-/-}$ mice compared to that of controls (Fig. 25A–C). $K6^{+}$ BPs are abundant at 4-6 weeks of age, gradually decreased with age, and finally disappeared after 12 weeks of age (Sun et al., 2010). Intriguingly, abundant $K6^{+}$ cells were still detected even in 14-month-old *Id2*$^{-/-}$ mice, while rarely detected in controls of the same age (Fig. 25A, B).

To further examine whether the increase of $K6^{+}$ BPs in *Id2*$^{-/-}$ ducts is due to continuous proliferation of $K6^{+}$ BPs, I conducted IHC for proliferating cell nuclear antigen (PCNA) and K6. Unexpectedly, however, most $K6^{+}$ cells in *Id2*$^{-/-}$ mice were PCNA-negative, whereas control mice were PCNA-positive (Fig. 26A, B). Consistently, cyclin-dependent kinase inhibitor 1B (CDKN1B or p27) was expressed in $K6^{+}$ cells of *Id2*$^{-/-}$ ducts, but not in controls (Fig. 27A). When I examined the expression levels of CDK inhibitors, *p15, p16, p21*, and *p27*, in the

$K6^+$ BP-enriched $CD61^-CD49b^-$ cells, the expressions of CDK inhibitors were dramatically increased in *Id2*$^{-/-}$ $K6^+$ BP-enriched $CD61^-CD49b^-$ cells compared to those of controls (Fig. 27B). Taken together, *Id2*$^{-/-}$ mice had accumulated aberrant $K6^+$ BPs, indicating that disruption of ID2 blocks the differentiation of $K6^+$ BPs into $CD61^+CD49b^+$ (hereafter $CD61^+$, since most of the $CD61^+$ cells were $CD49b^+$) LPs.

Figure 21. Accumulation of $K6^+$ BPs in *Id2*$^{-/-}$ ducts. (A–C) IHC staining for K6 and K8 with 8-week-old WT (A) and *Id2*$^{-/-}$ (B) mice, and quantification of ducts according to proportion of $K6^+$ cells in Hoechst-stained luminal cells (C). Most of WT ducts had no $K6^+$ cells (120/142), but over the half of *Id2*$^{-/-}$ ducts (107/205) had $K6^+$ cells. For quantification, I used two sides from each of three different mice. Scale bar, 100 μm; in the enlargements, 20 μm.

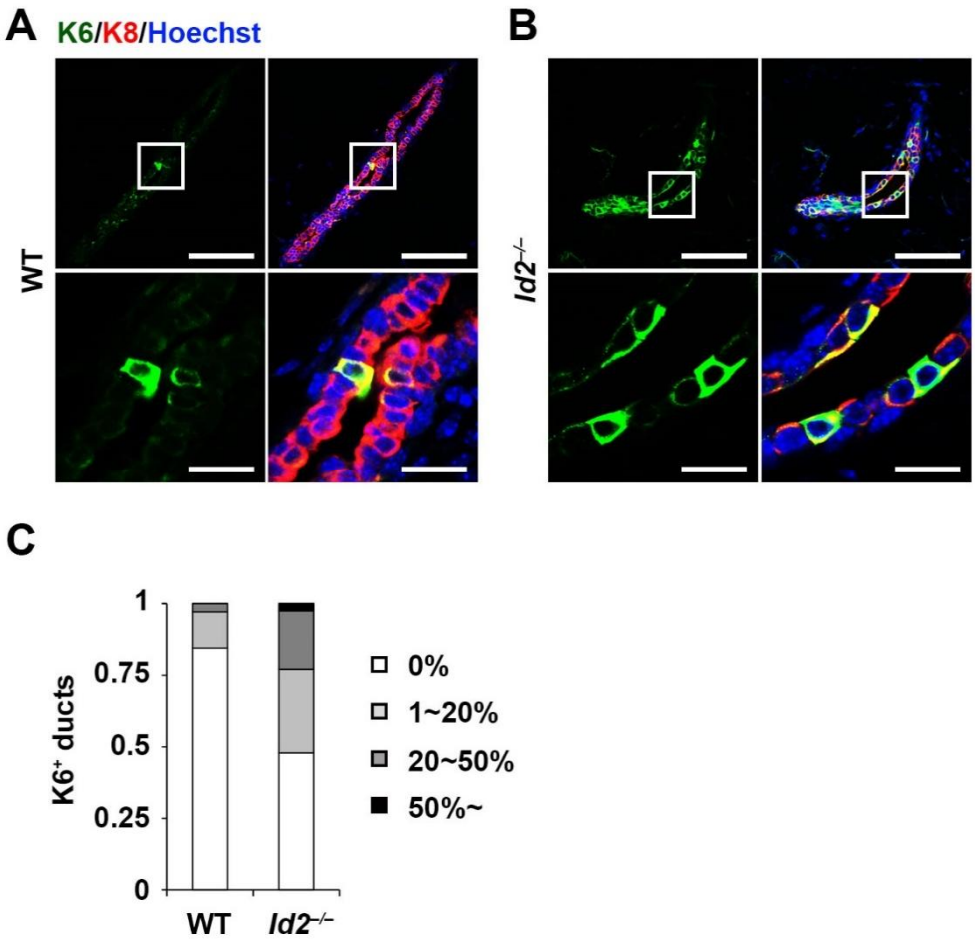
A
K6/K8/Hoechst
WT
B
Id2−/−
C
K6+ ducts
1
0.75
0.5
0.25
0
WT
Id2−/−
0%
1~20%
20~50%
50%~

Figure 22. Increased expression of K6 in *Id2*$^{-/-}$ ducts. (A, B) K6 expression in WT and *Id2*$^{-/-}$ mice, as determined by immunoblotting (A) and qRT-PCR (B). Deletion of ID2 resulted in increase of K6 expression. N=10, each. Data are means ± s.e.m.; Student's t tests. *p<0.05.

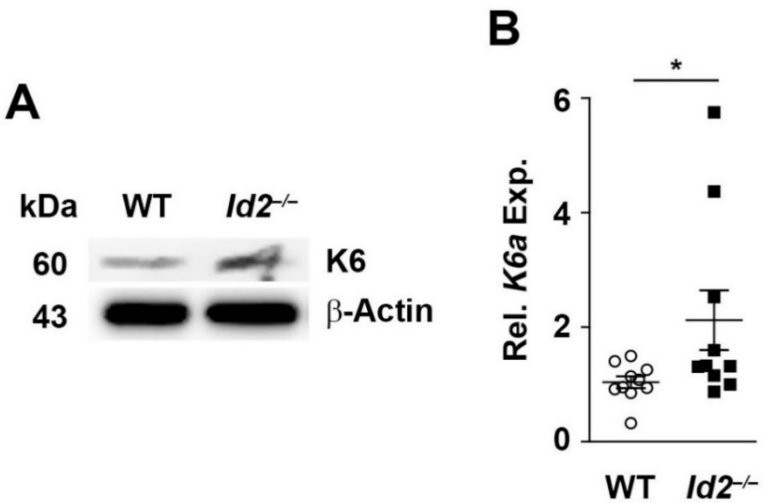
A
kDa
WT
Id2−/−
60
43
K6
β-Actin
B
*
Rel. K6a Exp.
6
4
2
0
WT
Id2−/−

Figure 23. Increase of $CD61^{-}CD49b^{-}$ luminal population in *Id2*$^{-/-}$ mice. (A) Schematic view for $CD61^{+}CD49b^{+}$ and $CD61^{-}CD49b^{-}$ population sorting with 6-week-old WT and *Id2*$^{-/-}$ mice. The plot was gated from the $CD29^{mid}CD24^{high}$ luminal population.

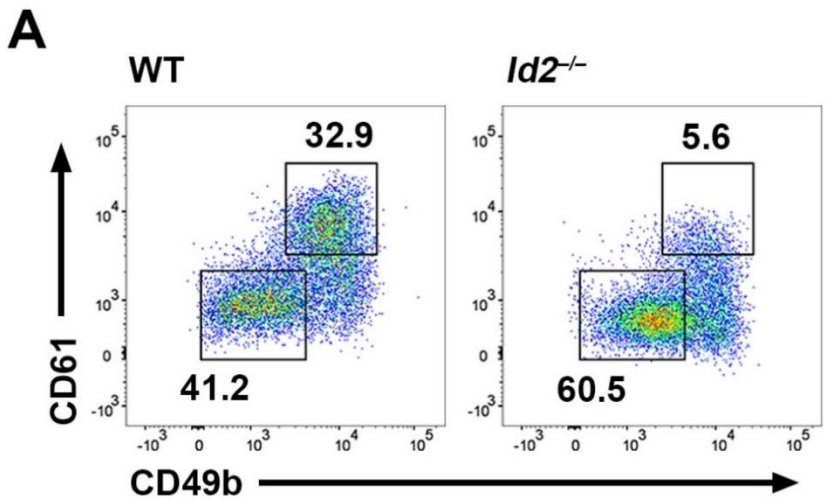
A
WT
Id2−/−
32.9
41.2
5.6
60.5
CD61
CD49b

Figure 24. High number of $K6^+$ BPs in $CD61^-CD49b^-$ luminal cells. (A, B) Immunocytochemistry (ICC) analysis for K6 with $CD61^+CD49b^+$ and $CD61^-CD49b^-$ luminal cells from 6-week-old WT mice (A), and proportion of $K6^+$ cells in each population (B). Most of $K6^+$ cells were found in $CD61^-CD49b^-$ luminal cells. Arrow, $K6^+$ cells with minimum fluorescence intensity. **(C)** qRT-PCR for *K6a* with $CD61^+CD49b^+$ and $CD61^-CD49b^-$ luminal cells from 6-week-old WT mice. $CD61^-CD49b^-$ luminal population showed increased *K6a* gene expression compared to $CD61^+CD49b^+$ luminal population. Scale bar, 30 μm. N=4, each. Data are means ± s.e.m.; Student's t tests. ***$p<0.001$

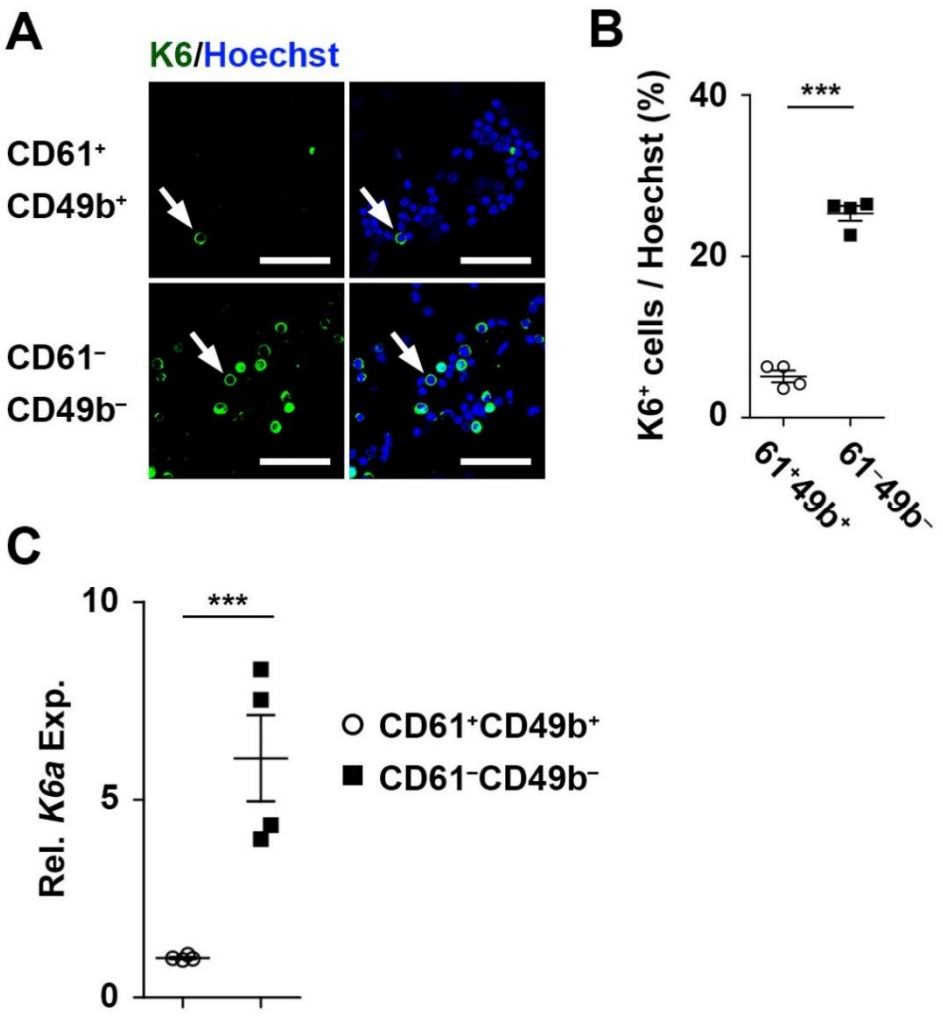
A
K6/Hoechst
CD61+
CD49b+
CD61−
CD49b−
B
K6+ cells / Hoechst (%)
40
20
0
***
61+49b+
61−49b−
C
Rel. K6a Exp.
10
5
0
***
CD61+CD49b+
CD61−CD49b−

Figure 25. High number of $K6^+$ BPs in $CD61^-CD49b^-$ luminal cells from *Id2*$^{-/-}$ mice. (A, B) ICC staining for K6 with $CD61^-CD49b^-$ luminal cells from 6- or >20-week-old WT and *Id2*$^{-/-}$ mice (A), and proportion of $K6^+$ cells in each population (B). While matured WT mice barely had $K6^+$ cells, old *Id2*$^{-/-}$ mice showed numerous $K6^+$ cells. I detected $K6^+$ cells even in 14 months of age *Id2*$^{-/-}$ mice. **(C)** qRT-PCR for *K6a* with $CD61^-CD49b^-$ luminal cells from 6-week-old WT and *Id2*$^{-/-}$ mice based on ICC staining. Scale bar, 30 μm. N=4, each. Data are means ± s.e.m.; Student's t tests. $^{**}p<0.01$.

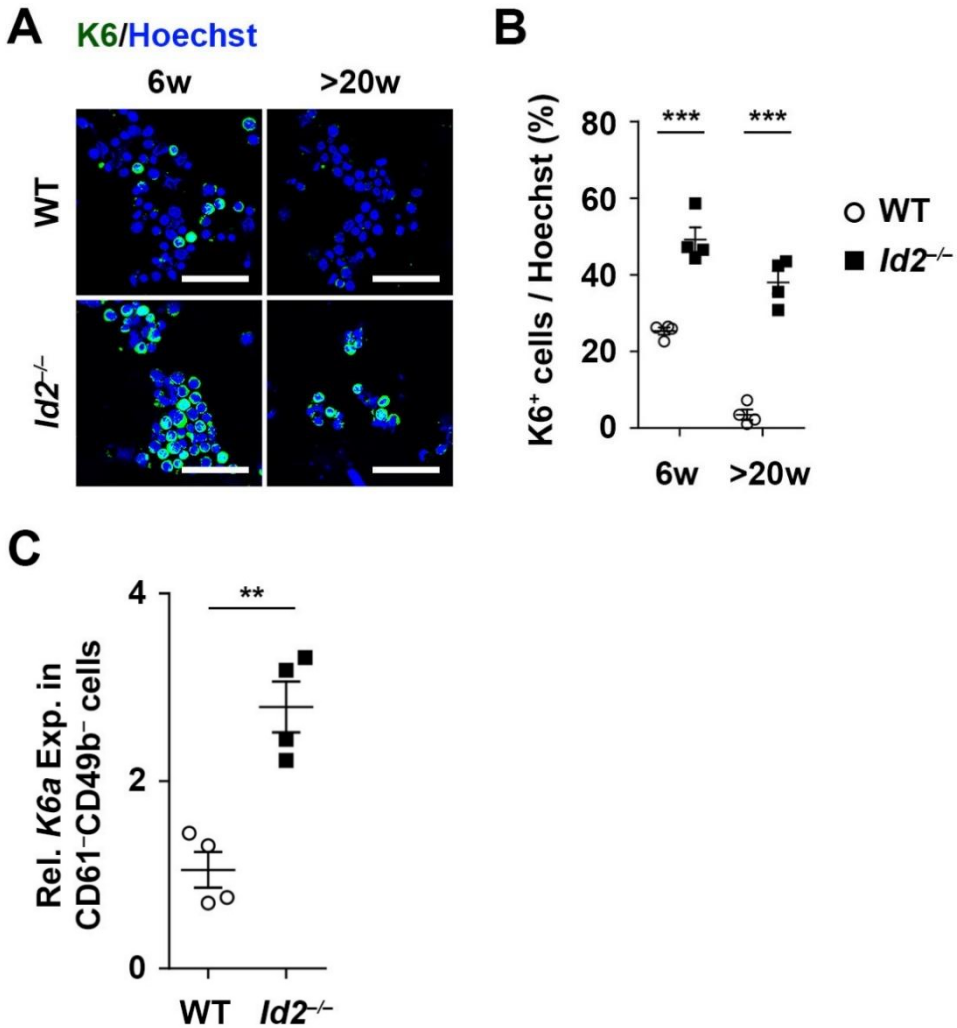
A
K6/Hoechst
6w
>20w
WT
Id2−/−
B
K6+ cells / Hoechst (%)
80
60
40
20
0
***
***
6w
>20w
WT
Id2−/−
C
Rel. K6a Exp. in CD61−CD49b− cells
4
2
0
**
WT
Id2−/−

Figure 26. Accumulation of aberrant $K6^+$ BPs by deletion of ID2. (A, B) IHC staining for K6 and PCNA of flattened mammary gland tissues from 6-week-old WT and *Id2*$^{-/-}$ mice (A), and quantification of $PCNA^+$ cells in $K6^+$ cells (B). To secure enough number of $K6^+$ cells, I used 6-week-old mice rather than 8-week-old mice for K6 studies. Although K6 represents bipotent progenitor cells, $K6^+$ cells in *Id2*$^{-/-}$ mice were not proliferative while most of $K6^+$ cells in WT mice entered cell cycle. Scale bar, 20 μm. N=4, each. Data are means ± s.e.m.; Student's t tests. ***p<0.001

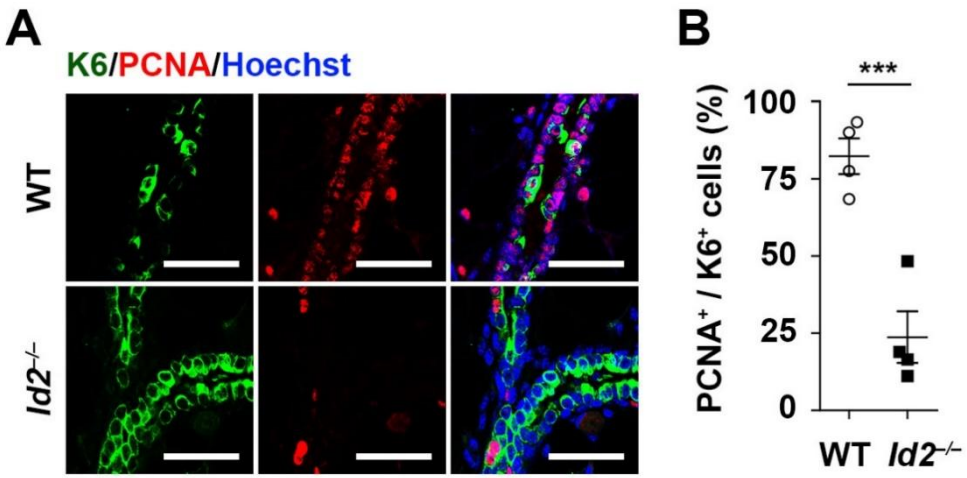
A
K6/PCNA/Hoechst
WT
Id2−/−
B
***
PCNA+ / K6+ cells (%)
100
75
50
25
0
WT
Id2−/−

Figure 27. Increase of cell cycle inhibitors in $K6^+$ BPs of *Id2*$^{-/-}$ mice. (A) IHC staining for K6 and p27 (cyclin-dependent kinase inhibitor 1B, CDKN1B) with flattened mammary gland tissues from 6-week-old *Id2*$^{-/-}$ mice. $K6^+$ cells in *Id2*$^{-/-}$ mice had p27 in nuclei while $K6^+$ cells in WT mice barely had p27. **(B)** qRT-PCR for cell cycle inhibitors with $CD61^-CD49b^-$ luminal cells from 6-week-old WT and *Id2*$^{-/-}$ mice. Dramatic increase of $K6^+$ bipotent progenitor cells without cell proliferation in *Id2*$^{-/-}$ mice indicates that ID2 is crucial for differentiation of $K6^+$ bipotent progenitor cells into $CD61^+$ luminal progenitor cells. Scale bar, 20 μm. N=4, each. Data are means ± s.e.m.; Student's t tests. **p*<0.05; ***p*<0.01; ****p*<0.001

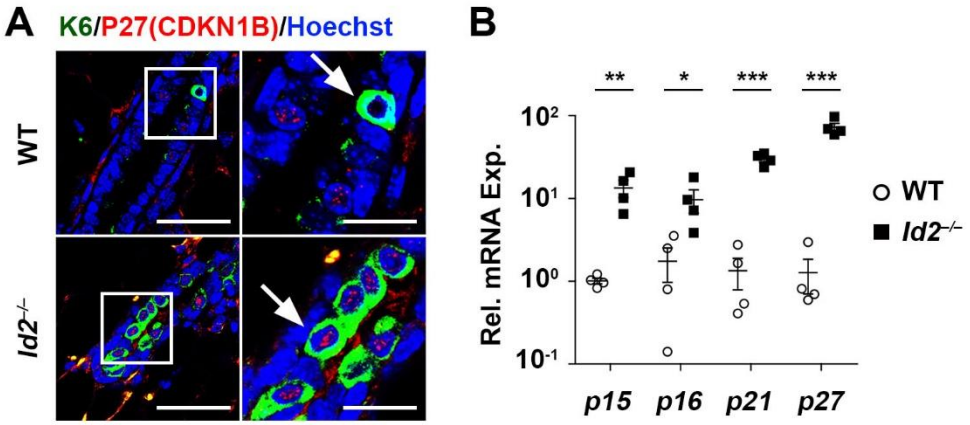
A
K6/P27(CDKN1B)/Hoechst
WT
Id2-/-
B
Rel. mRNA Exp.
10^2
10^1
10^0
10^-1
**
*
***
***
p15
p16
p21
p27
WT
Id2-/-

Differentiation of $K6^+$ BPs into $CD61^+$ LPs and side branch formation by nuclear ID2

To examine whether ID2 indeed induces the differentiation of $K6^+$ BPs into $CD61^+$ LPs, I transfected either hemagglutinin (HA)-tagged *Id2* or HA-nuclear localized sequence (NLS)-tagged *Id2* gene into HC11 cells, and conducted ICC analysis for HA and either K6 or CD61. Notably, the ectopic expression of *NLS-Id2* into HC11 cells resulted in the induction of $CD61^+$ cells while showing a significant reduction of $K6^+$ cell numbers in contrast to that of cells with *Id2* overexpression (Fig. 28A–C), in which the cells with cytosolic ID2 remained in $K6^+$ and $CD61^-$ (arrowhead), whereas the cells with nuclear ID2 resulted in $K6^-$ and $CD61^+$ (arrow). Even in *HA-Id2* vector transfected groups, the cells with nuclear ID2 were CD61-positive (data not shown). Consistently, overexpression studies using human mammary cell lines (MCF10A, MCF7, SK-BR3, HCC70, AU565) also showed the similar results (data not shown). Collectively, my data show that ID2, particularly nuclear ID2, strongly drives the differentiation of $K6^+$ BPs into $CD61^+$ LPs.

Next, to examine whether nuclear translocation of ID2 is crucial for side branching, our laboratory generated and I examined *MMTV-HA-NLS-Id2* Tg (*NLS-Id2* Tg) mice. *NLS-Id2* Tg mice showed 3.2-fold and 9.2-fold increased numbers of nascent/budding and side branches compared to those of controls, respectively (Fig. 29A, B). Intriguingly, although there was no difference in the numbers of primary and secondary ducts, *NLS-Id2* Tg mice showed slightly delayed primary ductal

elongation, which might be due to diverted resources used for drastic side branching induction. Indeed, 10-week-old *NLS-Id2* Tg mice showed normal length of primary ducts compared with those of control mice (data not shown).

To investigate whether nuclear ID2 indeed induces the differentiation of $K6^+$ BPs into $CD61^+$ LPs *in vivo*, I conducted IHC for HA, and either K6 or CD61, using *NLS-Id2* Tg mice. Notably, almost all HA^+ cells (the cells with overexpressed nuclear ID2) were $K6^-$ but $CD61^+$, consistent with *in vitro* data (Fig. 30A–C). Moreover, $CD61^+$ cells were observed at budding and side branches in *NLS-Id2* Tg mice similar to those of WT mice (Fig. 31A).

In H&E staining, *NLS-Id2* Tg mice seemed to have alveolus-like structures, even in virgin mice (Fig. 32A). To elucidate the characteristics of alveolus-like structures in *NLS-Id2* Tg mice, I examined the gene expression profiles of typical milk protein genes, such as *β-casein, Wap, α-lactalumin*. However, there was no significant induction of milk protein genes in *NLS-Id2* Tg mice compared with that in WT virgin mice (Fig. 32B). Moreover, alveolus-like structures in *NLS-Id2* Tg mice showed obviously different shapes from the alveoli of lactation day 1 (L1) mice (Fig. 32C), indicating that alveolus-like structures in *NLS-Id2* Tg mice are budding branches rather than milk-producing lobulo-alveoli. Taken together, my findings showed that *NLS-Id2* Tg mice had dramatically increased nascent/budding and side branches, and that nuclear ID2 induces luminal lineage commitment and formation of nascent/budding branches.

Figure 28. Induction of luminal lineage differentiation by nuclear ID2. (A–C) ICC staining for CD61, K6, and HA in HC11 cells transfected with HA-tagged *Id2*- or HA-tagged *NLS-Id2*- overexpressing vectors (A, B), and quantification of $K6^+$ or $CD61^+$ cells in HA-positive HC11 cells (C). The cells with nuclear ID2 showed significant reduction of K6 and induction of CD61 expression. HA^-CD61^+ cells might be $CD61^+$ cells which were differentiated by endogenous ID2 rather than ectopic ID2. Arrow, nuclear ID2; arrowhead, cytosolic ID2. Scale bar, 100 μm. N=4, each. For statistics, I counted at least 100 HA^+ cells for each data. Data are means ± s.e.m.; Student's t tests. ***p<0.001.

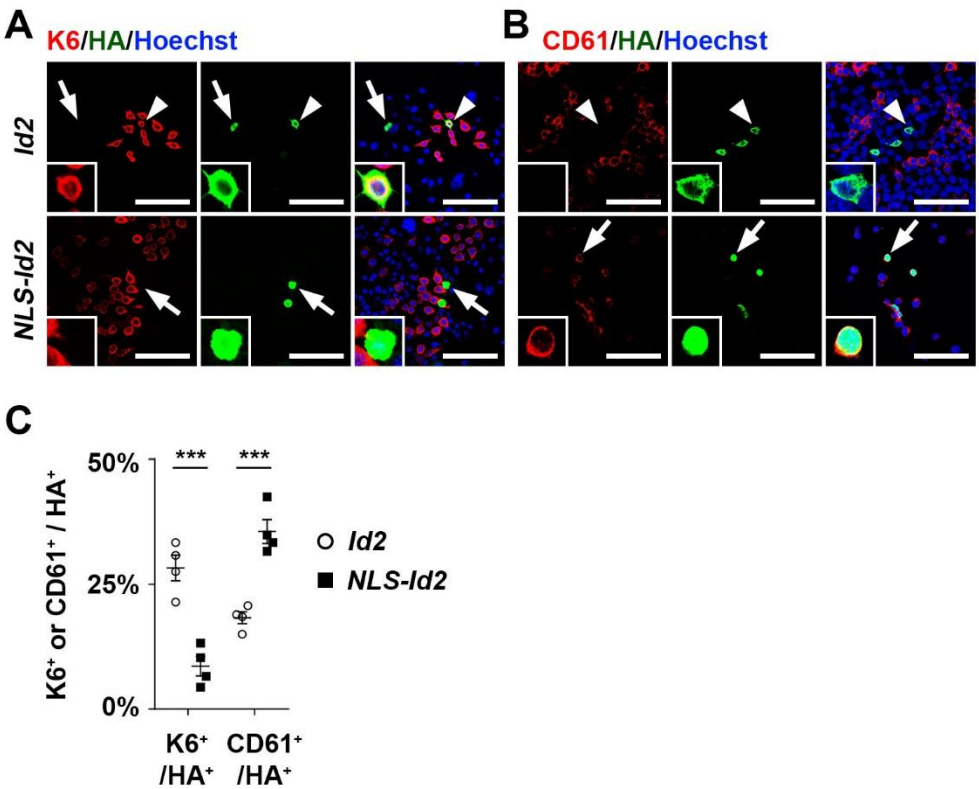
A
K6/HA/Hoechst
Id2
NLS-Id2
B
CD61/HA/Hoechst
C
50%
25%
0%
***
***
K6+ or CD61+ / HA+
Id2
NLS-Id2
K6+ /HA+
CD61+ /HA+

Figure 29. Induction of side branching by nuclear ID2. (A, B) C-A-stained inguinal mammary glands (A), and quantification of branches (B) in 8-week-old WT and *NLS-Id2* Tg mice. Overexpression of nuclear ID2 resulted in dramatic increase of side branches and nascent/budding branches. The circle indicates the nipple. 1', 2', 3', and N/B represent the primary duct, secondary branch, tertiary branch (terminal side branch), and nascent/budding branch, respectively. N=4, each. Scale bar, 1 cm; in the enlargements, 1 mm. Data are means ± s.e.m.; Student's t-tests. *p<0.05, ***p<0.001.

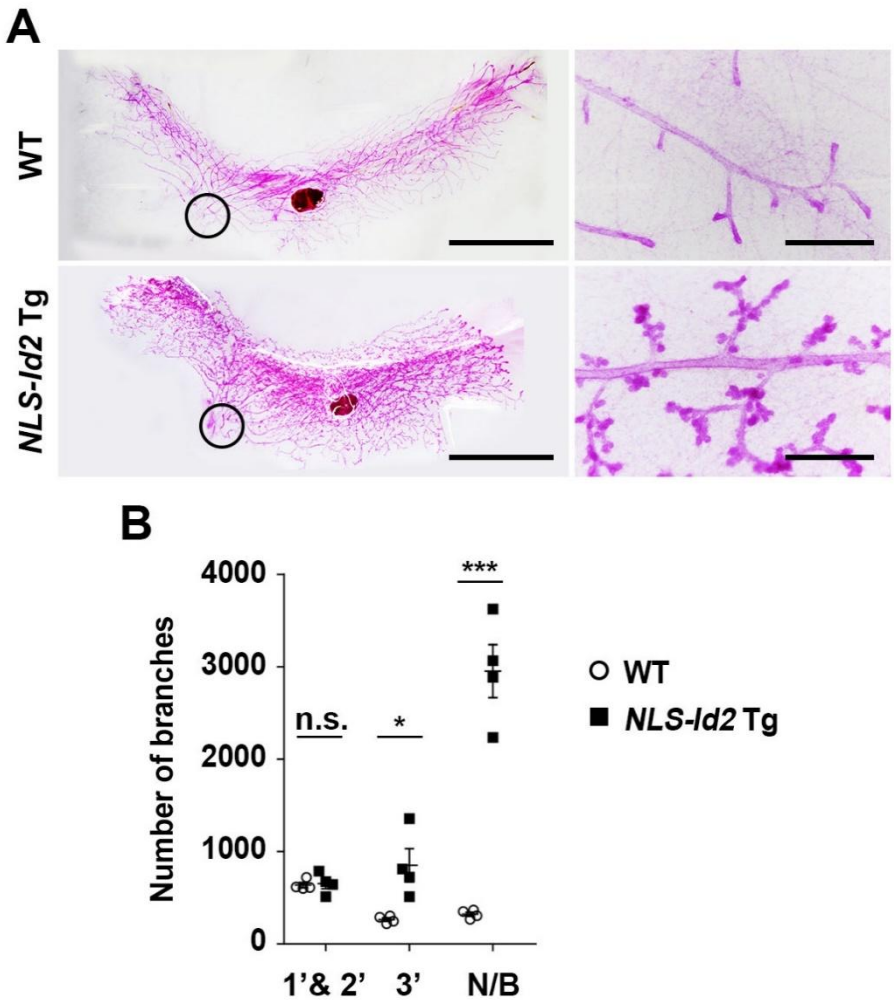
A
WT
NLS-Id2 Tg
B
Number of branches
4000
3000
2000
1000
0
n.s.
*
***
1'& 2'
3'
N/B
WT
NLS-Id2 Tg

Figure 30. Luminal lineage differentiation from $K6^+$ LPs into $CD61^+$ LPs by nuclear ID2. (A–C) IHC staining for HA, and either K6 or CD61 in 8-week-old *NLS-Id2* Tg mice (A, B) and quantification of $K6^+$ or $CD61^+$ cells in HA^+ cells (C). Luminal cells having nuclear ID2 did not express K6 ($K6^+$ / nuclear $ID2^+$ cells, 0.00%; $K6^+$ / whole luminal cells, 4.48% ± 1.69%) but did express CD61, suggesting that ID2 strongly differentiates $K6^+$ bipotent progenitor cells into $CD61^+$ luminal progenitor cells. Arrowhead, HA^+ cells. Scale bar, 20 μm. N=5, each. Data are the means ± s.e.m. Student's t-tests. ***p<0.001

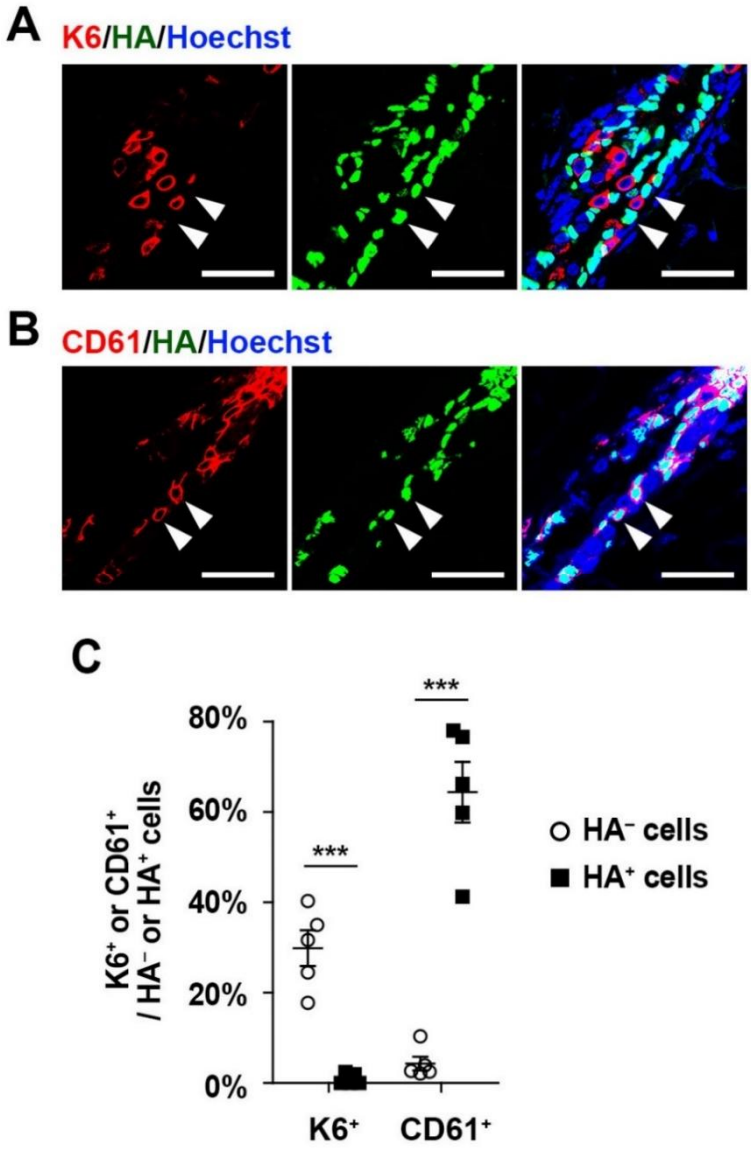
A
K6/HA/Hoechst
B
CD61/HA/Hoechst
C
***
***
80%
60%
40%
20%
0%
K6⁺ or CD61⁺
/ HA⁻ or HA⁺ cells
HA⁻ cells
HA⁺ cells
K6⁺
CD61⁺

Figure 31. CD61 expression in budding and side branches in NLS-Id2 Tg mice.

(A) IHC staining for CD61 and K8 in 8-week-old *NLS-Id2* Tg mice. $CD61^{+}$ cells were detected in nascent/budding branches rather than primary ducts. Arrowhead, budding branches. Scale bar, 100□m; in the enlargements, 20 μm.

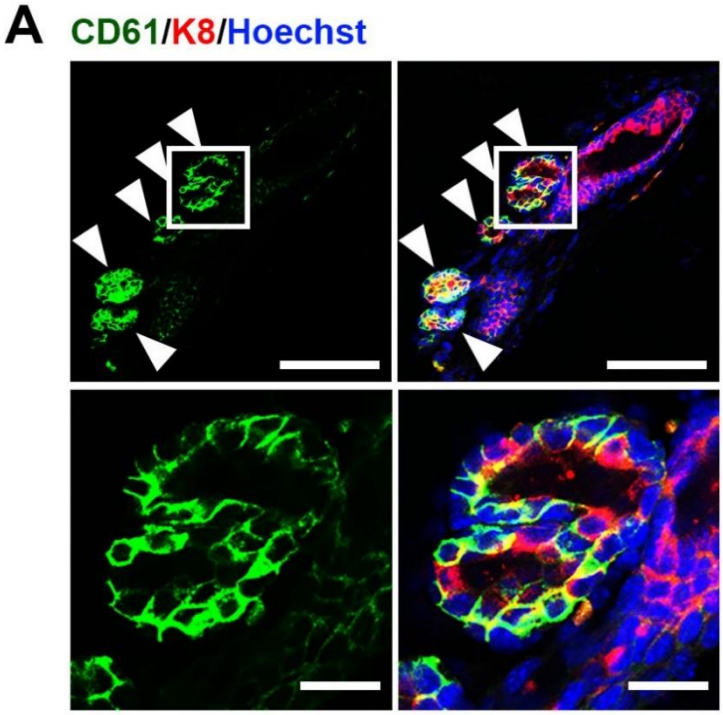
A
CD61/K8/Hoechst

Figure 32. Increased number of budding branches rather than alveoli in NLS-Id2 Tg mice. (A) H&E-stained mammary glands from 8-week-old *NLS-Id2* Tg mice. Arrowheads, nascent/budding branches. Scale bar, 200 μm. **(B)** qRT-PCR for milk protein genes in MECs from WT, *NLS-Id2* Tg, and lactation day 1 (L1, positive control) mice. WT (n=5), *NLS-Id2* Tg (n=3), L1 (n=3). Data are means ± s.e.m.; Student's t tests. *p<0.05; **p<0.01; ***p<0.001. **(C)** IHC staining for milk proteins and K8 in 8-week-old WT, *NLS-Id2* Tg, and 12-week-old lactation day 1 (L1) mice. The mammary gland tissues were precisely flattened for better imaging analysis. Alveoli-like structure in *NLS-Id2 Tg* mice were different from alveoli in L1 mice. Arrowhead, budding branches. Scale bar, 100 μm.

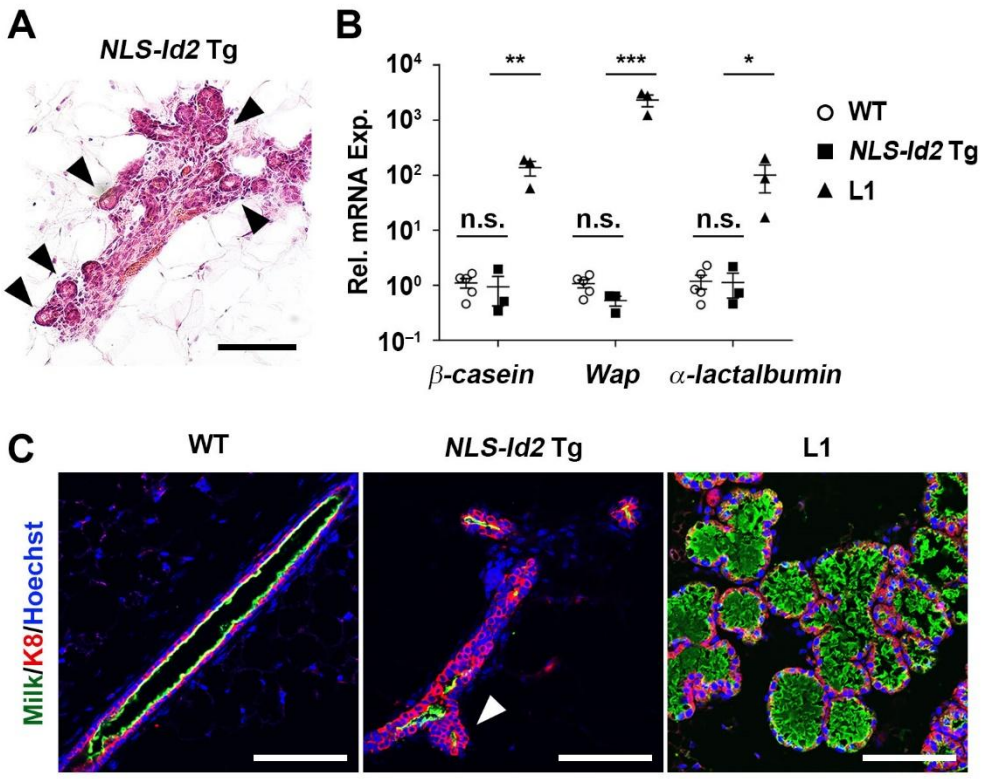
A
NLS-Id2 Tg
B
Rel. mRNA Exp.
10^4
10^3
10^2
10^1
10^0
10^−1
**
***
*
n.s.
n.s.
n.s.
β-casein
Wap
α-lactalbumin
WT
NLS-Id2 Tg
L1
C
WT
NLS-Id2 Tg
L1
Milk/K8/Hoechst

Nuclear ID2 as a key mediator of progesterone for side branching and differentiation into CD61^{+} LPs

Our laboratory previously reported that RANKL, a key mediator of progesterone signaling, induced nuclear retention of ID2 in lactating mammary glands (Kim et al., 2006; Kim et al., 2011), suggesting that ID2 nuclear localization may be induced by progesterone signaling. To investigate whether nuclear ID2 acts as a key mediator of progesterone for side branching, I performed ovariectomy (Ovx) in 5-week-old WT and *NLS-Id2* Tg mice, and administered 17β-estradiol with or without progesterone (Fig. 33A). I also prepared corn oil-administered Ovx groups as negative controls (Fig. 33B, E). Estradiol alone barely induced side branching in WT Ovx mice, whereas administration of 17β-estradiol with progesterone induced the formation of normal ductal trees (Fig. 33C, D). Notably, in *NLS-Id2* Tg Ovx mice, 17β-estradiol alone readily induced side branches, which were comparable to those in WT Ovx mice treated with both 17β-estradiol and progesterone (Fig. 33F). The administration of both 17β-estradiol and progesterone into *NLS-Id2* Tg Ovx mice showed comparable numbers of nascent/budding branches and side branches compared to those of 17β-estradiol alone (Fig. 33G and 34A), indicating that overexpression of nuclear ID2 can replace the function of progesterone. To demonstrate the overexpression of nuclear ID2 in the *NLS-Id2* Tg Ovx mice with 17β-estradiol treatment, I conducted IHC for HA with *NLS-Id2* Tg sham and Ovx mice administered with corn oil, 17β-estradiol, and both 17β-estradiol and

progesterone. I found that nuclear ID2 was overexpressed in all hormone-treated groups (Fig. 35A, B). Taken together, my results show that nuclear ID2 is a key mediator of progesterone signaling which induces new side branches.

Progesterone is essential for terminal differentiation of luminal cells (Beleut et al., 2010; Lee et al., 2013) as well as side branching. To investigate whether nuclear ID2 also plays a role in luminal differentiation as a mediator of progesterone signaling, I performed ovariectomy in 3-week-old WT and *NLS-Id2* Tg mice and administered 17β-estradiol with or without progesterone (Fig. 36A). WT Ovx mice treated with 17β-estradiol showed decreased populations of $CD29^{mid}CD24^{high}$ luminal cells and $CD61^{+}$ LPs compared with sham groups, and WT Ovx mice treated with both 17β-estradiol and progesterone rescued the impaired luminal lineage differentiation (Fig. 36B, C), indicating that progesterone induces luminal lineage differentiation. Importantly, in *NLS-Id2* Tg Ovx mice, 17β-estradiol alone substantially induced the differentiation of luminal lineage cells comparable to sham groups (Fig. 36B, C). These data indicate that nuclear ID2 overexpression is sufficient to induce luminal lineage differentiation, even without progesterone.

To confirm whether ID2 is a mediator of progesterone signaling in the differentiation of luminal lineage cells, I conducted flow cytometry with $Id2^{-/-}$ Ovx mice after treatment with 17β-estradiol alone or with both 17β-estradiol and progesterone. Both groups of $Id2^{-/-}$ Ovx mice showed impaired $CD29^{mid}CD24^{high}$

luminal and $CD61^+$ LP populations (Fig. 37A). Progesterone barely induced the differentiation of $CD61^+$ LPs without ID2, indicating that ID2 is a key mediator of progesterone signaling for luminal lineage differentiation.

Figure 33. Nuclear ID2 as a key mediator of progesterone signaling for side branching. (A) Schematic timeline for ovariectomy and hormone administration to examine the effects of ID2 on side branching. For side branching analysis, ovariectomy was performed in 5-week-old WT and *NLS-Id2* Tg mice in order to avoid confusion of newly formed side branches induced by ID2 from natural side branches induced by endogenous hormones, because endogenous side branches were evident in 6-week-old WT virgin mice. Three weeks after ovariectomy, 17β-estradiol with or without progesterone was administered for 1 week. **(B–G)** C-A-stained inguinal mammary glands from ovariectomized 5-week-old WT and *NLS-Id2* Tg Ovx mice treated with corn oil, 17β-estradiol and progesterone. Both negative control groups showed shrunk TEBs and rare side branches. WT Ovx mice treated with 17β-estradiol alone had only few side branches, whereas WT Ovx mice treated with both 17β-estradiol and progesterone showed considerable nascent/budding and side branches. Importantly, *NLS-Id2* Tg Ovx mice treated with 17β-estradiol alone showed numerous side branches. C, corn oil; E2, 17β-estradiol; EP, 17β-estradiol and progesterone administration. Scale bar, 5 mm; in the enlargements, 0.5 mm.

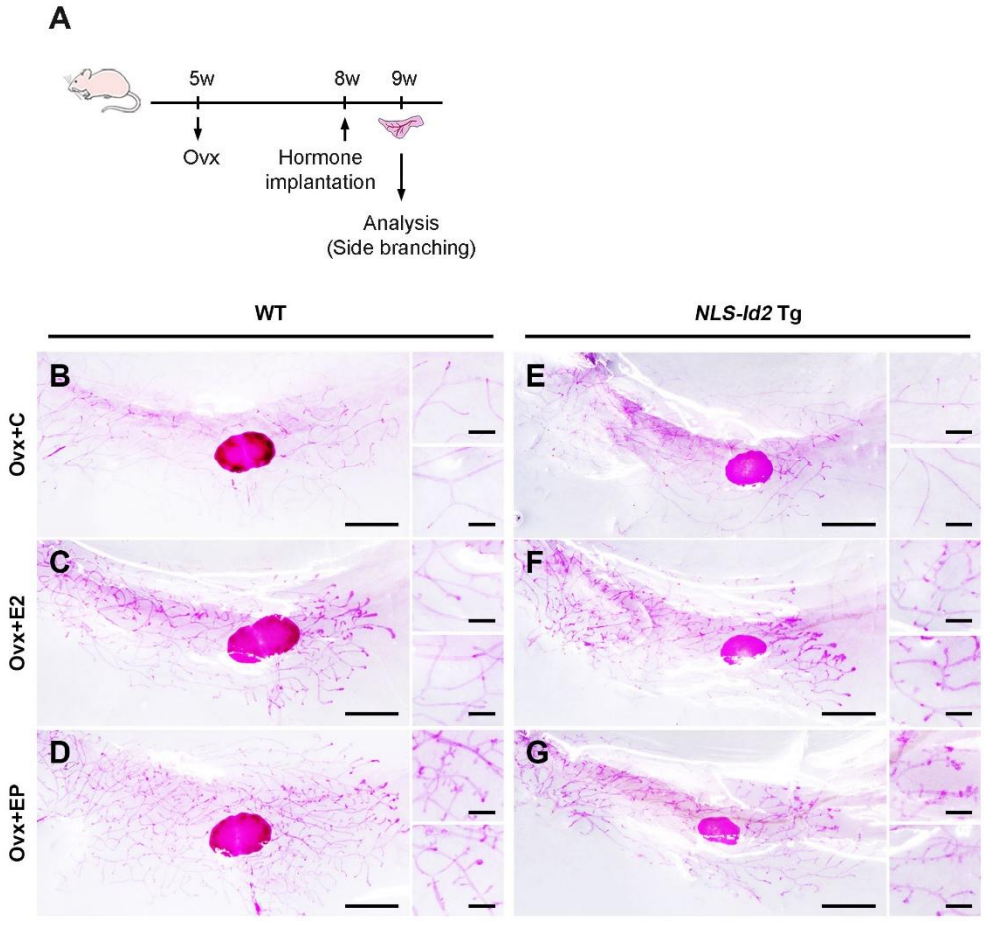
A
5w
8w
9w
Ovx
Hormone implantation
Analysis (Side branching)
WT
NLS-Id2 Tg
Ovx+C
Ovx+E2
Ovx+EP
B
C
D
E
F
G

Figure 34. Induction of side branch formation with ectopic ID2 alone without progesterone. (A) Numbers of branches in WT and *NLS-Id2* Tg Ovx mice based on C-A staining (Fig. 33B–G). WT sham mice were additionally analyzed as a control. N/B, nascent/budding branches. N=4, each. Data are means ± s.e.m.; two-way ANOVA analysis and student's t tests. $^{**}p<0.01$.

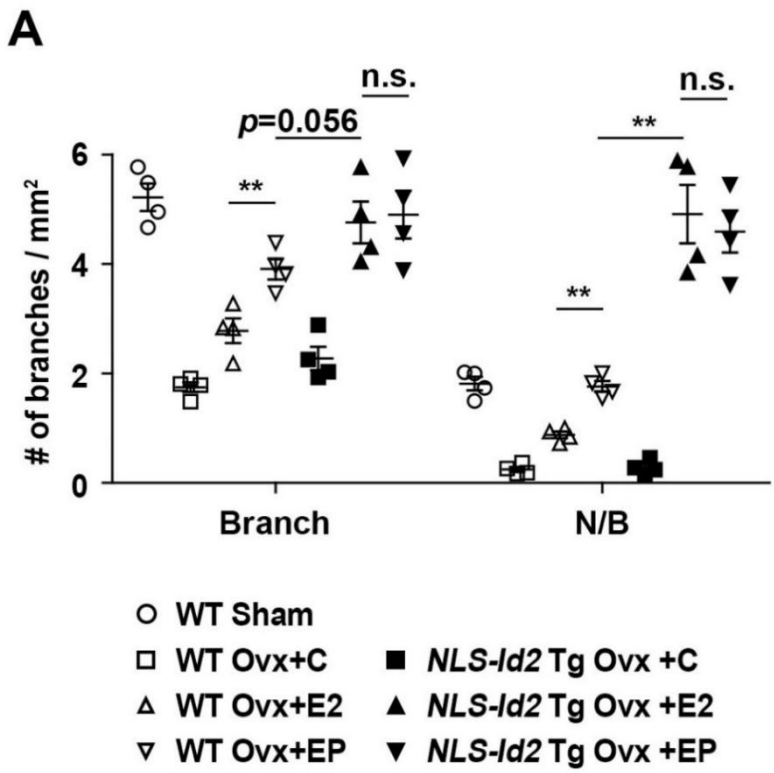
A
n.s.
n.s.
p=0.056
**
**
**
6
4
2
0
# of branches / mm²
Branch
N/B
WT Sham
WT Ovx+C
WT Ovx+E2
WT Ovx+EP
NLS-Id2 Tg Ovx +C
NLS-Id2 Tg Ovx +E2
NLS-Id2 Tg Ovx +EP

Figure 35. Activation of MMTV-promoter through injection of 17β-estradiol. **(A, B)** IHC staining for HA in 8-week-old *NLS-Id2* Tg Ovx mice (A) and quantification of HA^+ cells in Hoechst-stained luminal cells (B). Ectopic 17β-estradiol administration is sufficient to induce overexpression of nuclear ID2 in *NLS-Id2* Tg Ovx mice. Scale bar, 50 μm. Data are means ± s.e.m.; Student's t tests. ***$p<0.001$.

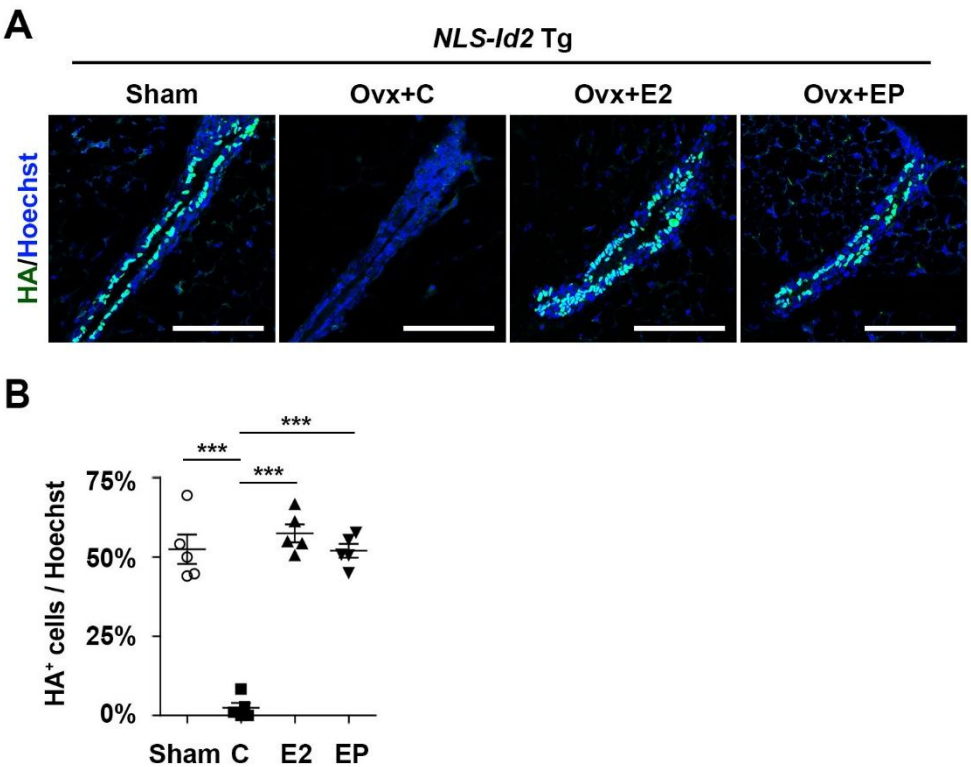
A
NLS-Id2 Tg
Sham
Ovx+C
Ovx+E2
Ovx+EP
HA/Hoechst
B
***
***
***
75%
50%
25%
0%
HA+ cells / Hoechst
Sham
C
E2
EP

Figure 36. Nuclear ID2 as a key mediator of progesterone signaling for luminal lineage differentiation. (A) Schematic timeline for ovariectomy and hormone administration to examine the effects of ID2 on luminal lineage differentiation. For analysis of luminal lineage differentiation, ovariectomy was performed at 3 weeks of age, at which point ductal elongation and cellular differentiation begin to occur through functions of ovarian hormones. Since I ovariectomized and treated hormones before endogenous ductal elongation was detected, resultant ductal elongation was due to implanted hormones. Three weeks after ovariectomy, 17β-estradiol with or without progesterone was administered for 3 weeks. **(B)** Flow cytometric analysis of $CD29^{mid}CD24^{high}$ luminal population upon hormone administration. The CD29-CD61 plot was gated from the $CD29^{mid}CD24^{high}$ luminal population. When given only 17β-estradiol, *NLS-Id2* Tg Ovx mice showed normal differentiation of luminal lineage cells, while WT Ovx showed reduced $CD29^{mid}CD24^{high}$ luminal and $CD61^{+}$ LP population. In WT Ovx mice, both 17β-estradiol and progesterone administration could not rescue luminal lineage differentiation completely, might be due to imbalance between ectopic 17β-estradiol and progesterone unlike physiological levels. **(C)** Quantification of the $CD61^{+}$ luminal progenitor population in whole MECs based on flow cytometry data. N=4, each. Data are means ± s.e.m.; two-way ANOVA analysis and student's t tests. $^{**}p<0.01$.

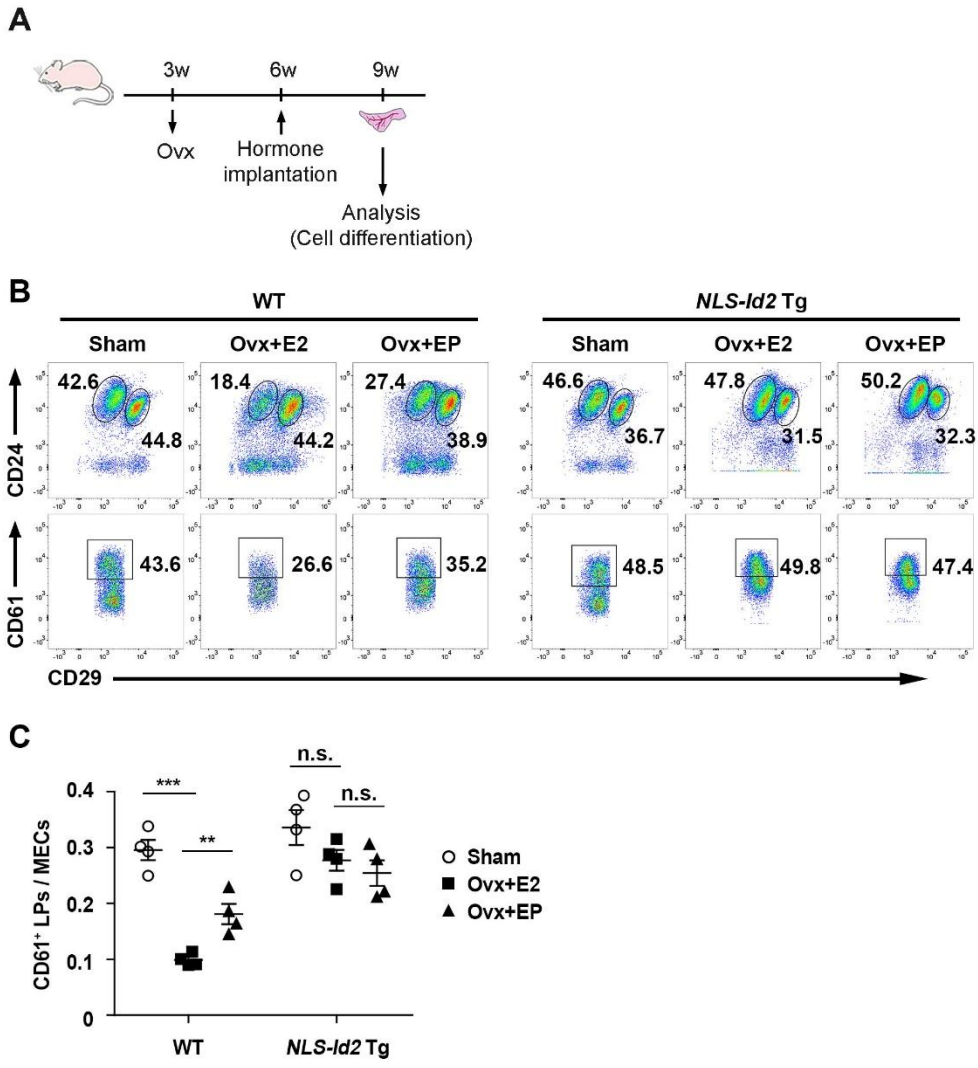
A
3w
6w
9w
Ovx
Hormone implantation
Analysis (Cell differentiation)
B
WT
NLS-Id2 Tg
Sham
Ovx+E2
Ovx+EP
CD24
CD61
CD29
42.6
44.8
18.4
44.2
27.4
38.9
46.6
36.7
47.8
31.5
50.2
32.3
43.6
26.6
35.2
48.5
49.8
47.4
C
CD61+ LPs / MECs
0.4
0.3
0.2
0.1
0
***
**
n.s.
n.s.
WT
NLS-Id2 Tg
Sham
Ovx+E2
Ovx+EP

Figure 37. ID2 as a key mediator of progesterone for luminal lineage differentiation. (A) Flow cytometric analysis with ovariectomized *Id2*$^{-/-}$ mice treated with 17β-estradiol with or without progesterone. The CD29-CD61 plot was gated from the CD29^{mid}CD24^{high} luminal population. Progesterone could not induce luminal lineage differentiation without ID2. E2, 17β-estradiol; EP, 17β-estradiol and progesterone administration.

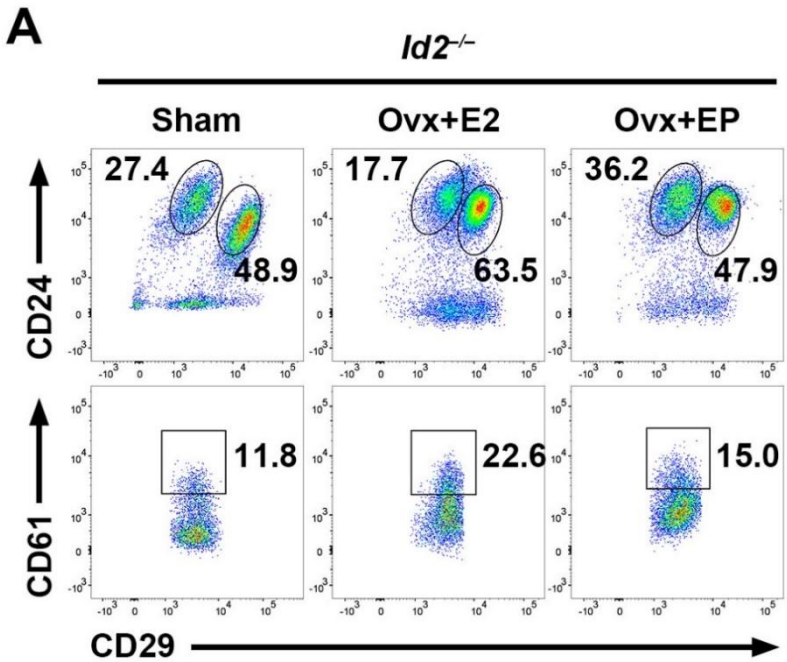
A
Id2−/−
Sham
Ovx+E2
Ovx+EP
27.4
48.9
17.7
63.5
36.2
47.9
CD24
11.8
22.6
15.0
CD61
CD29

Failure of CD61$^+$ LP-derived tumor formation in *Id2*$^{-/-}$ mice

MMTV-active Neu transgenic (*Neu* Tg) mouse is a widely used model for investigating luminal progenitor-derived tumors (Lo et al., 2012; Prat and Perou, 2009; Vaillant et al., 2008). As reported, tumor tissues (T) in *Neu* Tg mice (*Neu*_T) displayed high levels of *K8* and *Cd61*, but almost no *K14* (Vaillant et al., 2008) (Fig. 42A, C–E). Flow cytometry analysis also revealed that tumor tissues were composed of CD61$^+$ LPs (Fig. 38B). Along with increased *Cd61* expression, the dramatically decreased *K6a* expression (Fig. 38F) indicates that NEU strongly drives the differentiation of K6$^+$ BPs into CD61$^+$ LPs.

To prove that ID2 induces the generation of functional CD61$^+$ LPs rather than merely *Cd61* expression, I crossed *Id2*$^{-/-}$ mice with *Neu* Tg mice and hypothesized that LP-derived tumors will not be established in *Neu* Tg;*Id2*$^{-/-}$ mice if there is no cellular source for tumor occurrence. Importantly, I could not find any sign of tumors in *Neu* Tg;*Id2*$^{-/-}$ mice until 70-week-old, whereas all *Neu* Tg and *Neu* Tg;*Id2*$^{+/-}$ mice developed CD61$^+$ LP-derived tumors before 55-week-old (Fig. 39A). C-A staining also showed no occurrence of microtumors and even foci in *Neu* Tg;*Id2*$^{-/-}$ mice (Fig. 39B). Flow cytometry analysis showed markedly decreased populations of CD29^{mid}CD24^{high} luminal cells and CD61$^+$ LPs in *Neu* Tg;*Id2*$^{-/-}$ mice, despite intact expression of *Neu* (Fig. 39C, and data not shown). qRT-PCR and western blotting also showed that the expression levels of CD61, K8, and K18 were decreased in *Neu* Tg;*Id2*$^{-/-}$ mice compared with those in non-tumor

tissues (NT) from *Neu* Tg mice (*Neu*_NT), whereas K6 was increased (Fig. 40A–E). *Neu* Tg;*Id2*$^{-/-}$ mice did not show any decrease in NEU target genes, indicating that loss of ID2 does not affect NEU signaling (Fig. 41A). Collectively, without ID2, NEU barely drove differentiation of K6^{+} BPs into CD61^{+} LPs and could not induce LP-derived tumors, indicating that ID2 is essential for the differentiation of K6^{+} BPs into functional CD61^{+} LPs.

Figure 38. Characteristics of the tumor region of Neu Tg mice. (A) Optic image of tumors formed in 30-week-old *Neu* Tg mice. The red circle indicates the tumor. **(B)** Flow cytometric analysis of tumor (T) tissues from 28–32-week-old *Neu* Tg mice (*Neu*_T). Tumor tissues from *Neu* Tg mice were driven from $CD61^{+}$ luminal progenitor cells. CD29-CD61 plots were gated from the $CD29^{mid}CD24^{high}$ luminal population. **(C–F)** mRNA expression levels of mature luminal (C), myoepithelial (D), and progenitor markers (E, F) in WT MECs and tumor (T) tissues of *Neu* Tg MECs (*Neu*_T). Tumor tissues of *Neu* Tg MECs showed greatly increased luminal lineage marker expression (*Cd61, K8*) but dramatically decreased bipotent progenitor marker expression (*K6a*), suggesting that NEU mainly targets $K6^{+}$ bipotent progenitor cells and strongly drives differentiation of them into $CD61^{+}$ luminal progenitor cells for LP-derived tumor occurrence. *Neu* indicates *Neu* Tg mice. WT (n=5), *Neu*_T (n=4). Data are means ± s.e.m.; Student's t tests. $^{**}p<0.01$; $^{***}p<0.001$.

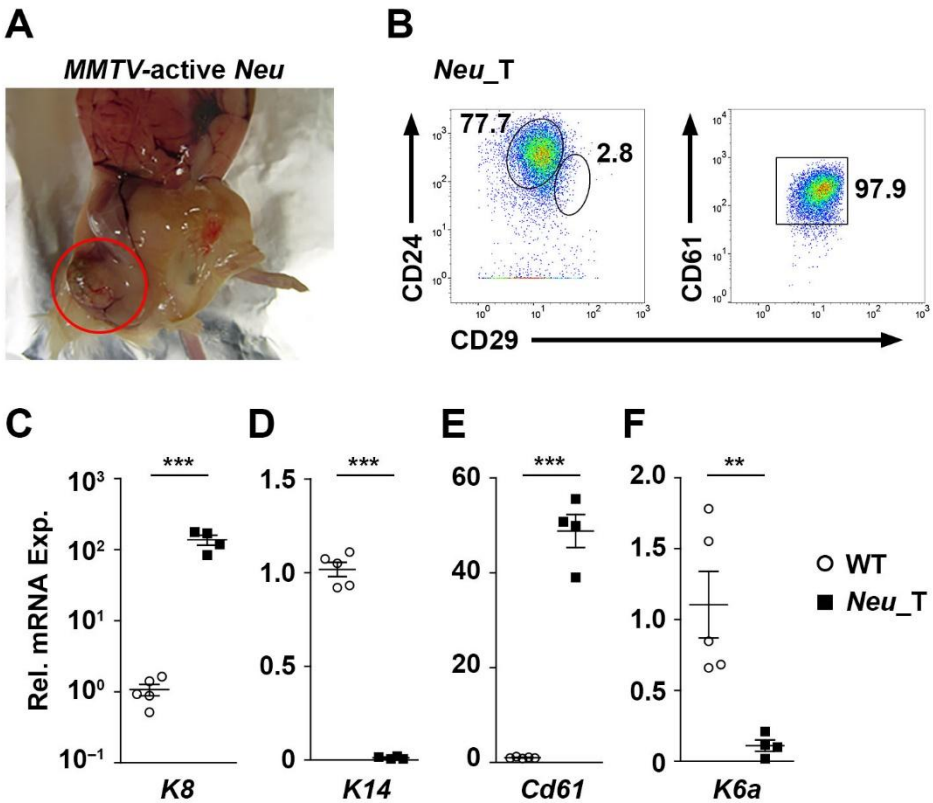
A
MMTV-active Neu
B
Neu_T
77.7
2.8
97.9
CD24
CD61
CD29
C
D
E
F
***
***
***
**
Rel. mRNA Exp.
K8
K14
Cd61
K6a
WT
Neu_T

Figure 39. Lack of CD61^{+} LP-derived tumors in *Id2*$^{-/-}$ mice. (A) Percentage of tumor-free mice at the indicated ages. *Neu* Tg or *Neu* Tg*;Id2*$^{+/-}$ (n=30); *Neu* Tg*;Id2*$^{-/-}$ (n=16). **(B)** C-A-stained inguinal mammary glands from 28–32-week-old WT and *Neu* Tg mice (E-H) and 70-week-old *Neu* Tg*;Id2*$^{-/-}$ mice (I and J). Along with reduction of side branches, *Neu* Tg*;Id2*$^{-/-}$ mice did not show any sign of tumors. Arrow, tumor or foci. Scale bar, 1 cm; in the enlargements, 1 mm. **(C)** Flow cytometric analysis of non-tumor (NT) tissues from 28–32-week-old *Neu* Tg mice (*Neu*_NT) and *Neu* Tg*;Id2*$^{-/-}$ mice. The slight increases in CD61^{+} LPs in non-tumor tissues from *Neu* Tg mice (*Neu*_NT) might be due to invisible microadenoma or hyperplastic luminal cells. CD29-CD61 plots were gated from the CD29^{mid}CD24^{high} luminal population. *Neu* indicates *Neu* Tg mice.

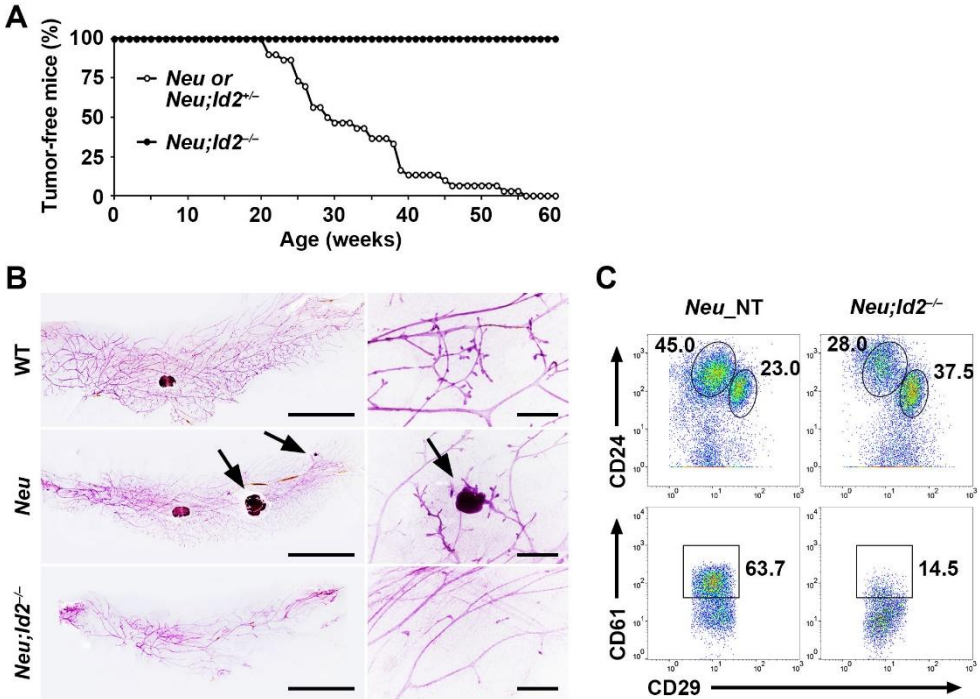
A
Tumor-free mice (%)
100
75
50
25
0
Neu or
Neu;Id2+/-
Neu;Id2-/-
0
10
20
30
40
50
60
Age (weeks)
B
WT
Neu
Neu;Id2-/-
C
Neu_NT
Neu;Id2-/-
45.0
23.0
28.0
37.5
CD24
63.7
14.5
CD61
CD29

Figure 40. Reduction of expression of luminal lineage markers in *Neu Tg;Id2*$^{-/-}$ mice. (A–D) qRT-PCR and **(E)** immunoblotting were used to analyze the expression of mature luminal (A), myoepithelial (B), and progenitor markers (C, D) in *Neu* Tg MECs isolated from non-tumor tissues (*Neu*_NT) and *Neu* Tg*;Id2*$^{-/-}$ MECs. Dramatic reduction of luminal lineage markers with increase of bipotent cell marker in *Neu* Tg*;Id2*$^{-/-}$ MECs indicates that loss of ID2 blocks differentiation of $K6^{+}$ bipotent progenitor cells into luminal lineage cells. *Neu* indicates *Neu* Tg mice. N=5, each. Data are means ± s.e.m.; Student's t tests. $^{**}p<0.01$; $^{***}p<0.001$.

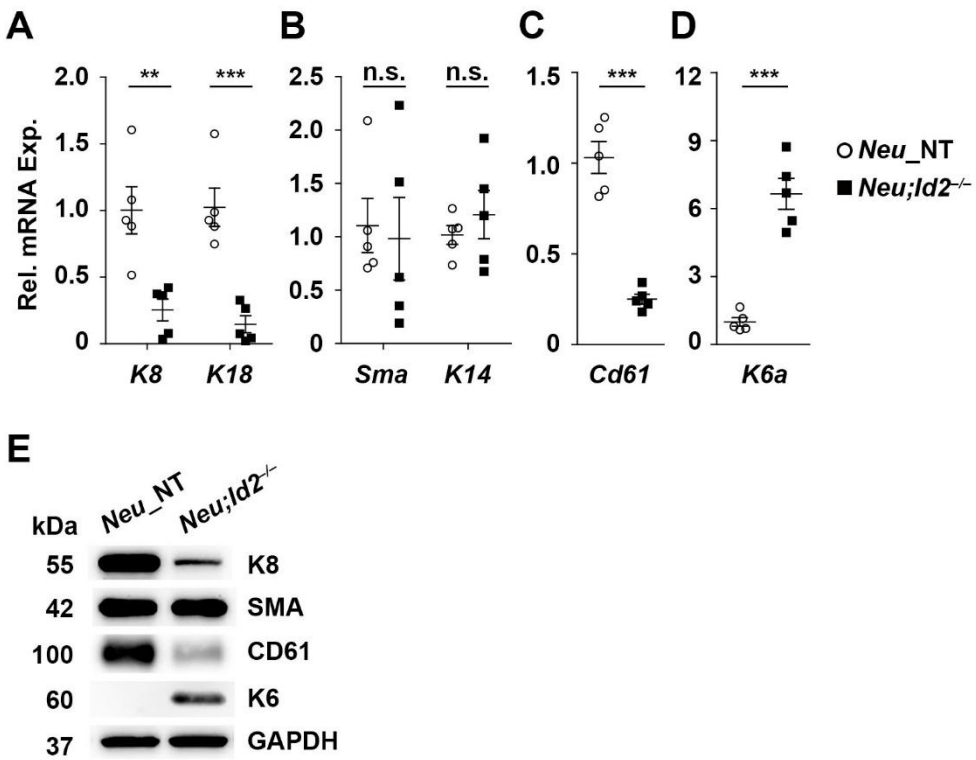
A
B
C
D
Rel. mRNA Exp.
2.0
1.5
1.0
0.5
0
**
***
K8
K18
2.5
2.0
1.5
1.0
0.5
0
n.s.
n.s.
Sma
K14
1.5
1.0
0.5
0
***
Cd61
12
9
6
3
0
***
K6a
Neu_NT
Neu;Id2−/−
E
kDa
Neu_NT
Neu;Id2−/−
55
K8
42
SMA
100
CD61
60
K6
37
GAPDH

Figure 41. Comparable expression of NEU target genes in *Neu Tg;Id2*$^{-/-}$ mice. **(A)** qRT-PCR analysis of the expression of NEU target genes. Non-tumor (NT) tissues from *Neu* Tg MECs (*Neu*_NT) and *Neu* Tg;*Id2*$^{-/-}$ MECs showed comparable expression of typical NEU target genes, indicating that ID2 is not a key mediator of NEU signaling. *Neu* indicates *Neu* Tg mice. N=3, each. Data represent the means ± s.e.m.

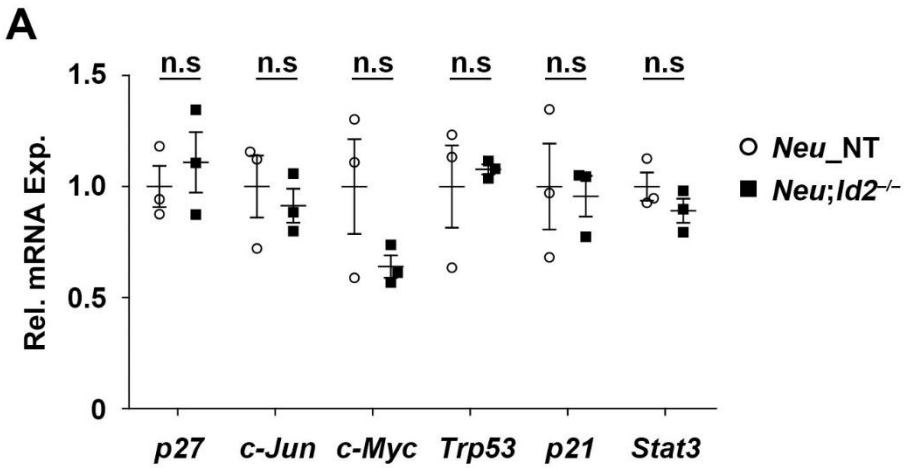
A
n.s
n.s
n.s
n.s
n.s
n.s
1.5
1.0
0.5
0
Rel. mRNA Exp.
p27
c-Jun
c-Myc
Trp53
p21
Stat3
Neu_NT
Neu;Id2-/-

DISCUSION

Mammary glands are essential for nursing offspring in mammals. In order to produce sufficient amount of milk, mammary glands overcome the spatial restriction of mammary epithelium in fat pads through side branching, like trees of the trachea in the lung. Previous studies revealed that ID2 is necessary for proper lobulo-alveologenesis during pregnancy, but the target cells and mechanism of action of ID2 has remained unsolved. In this study, I found that ID2 is crucial for side branching but not for primary ductal elongation, and that nuclear ID2 strongly drives differentiation of $K6^+$ BPs into $CD61^+$ LPs in budding side branches. Importantly, ovariectomy and hormone reconstitution studies revealed that nuclear ID2 drives side branching and luminal differentiation even without progesterone. Taken together, my findings suggest that ID2, as a mediator of progesterone, regulates side branching through inducing the differentiation of $CD61^+$ LPs at putative side branching points (Fig. 42A, B).

Recently, using *Rosa-confetti* mice, Scheele *et al.* reported that the bifurcation of TEBs is determined probabilistically (Scheele et al., 2017) and that branching occurs nearly exclusively through TEB bifurcation but not through side branching. Their observation was based on comparison of the branch length distributions between ductal trees of 5-week-old and 8-week-old mice and EdU incorporation assay, in which proliferation activity was only detected in TEBs but not in existing ducts. The same group also reported the mechanism of ductal

morphogenesis using the same model, in which EdU positive signals were detected even in existing ducts of proximal region near the nipple (Hannezo et al., 2017), suggesting that *de novo* side branching may occur independently from the bifurcation of TEBs. Indeed, many studies reported the existence of side branching. When primary ducts reach the end of the fat pad, TEBs terminate proliferation and lose their structure. Upon pregnancy, however, numerous side branches occur at the existing ducts (Brisken, 2013). Furthermore, progesterone administration into adult female mice results in increase of side branches without induction of primary elongation or bifurcation of TEBs (Atwood et al., 2000). Sale *et al.* reported that tertiary side branches were detected only in the proximal region but not in the distal region (Sale et al., 2013). Recently, Visvader group also reported that putative mammary stem cells reside mainly in the proximal region rather than in TEBs (Fu et al., 2017), suggesting the existence of stem/progenitor cells in the proximal region for side branches. Although Scheele and Hannezo *et al.* clearly demonstrated how bifurcation of TEB occurs to form primary and secondary ducts, the mechanism by which side branches are formed still needs to be investigated. Here, I report how side branches occur independently from primary ductal elongation.

Progesterone induces side branch formation by secreting paracrine mediators, such as RANKL, to neighboring $RANK^+$ cells (Beleut et al., 2010; Fernandez-Valdivia et al., 2009; Grimm et al., 2016; Lee et al., 2013; Mukherjee et al., 2010; Obr et al., 2013; Rajaram et al., 2015), suggesting that PGR^+ cells are

located near putative side branch points. However, PGR is not specifically detected in budding branches but widely distributed throughout ducts (Rajaram et al., 2015) (data not shown). Therefore, identifying the characteristics of $RANK^+$ cells may provide clues in elucidating the side branching mechanism by progesterone. In this study, I suggested that nuclear ID2 in $K6^+$ BPs is crucial for side branching and luminal lineage differentiation, and previously reported that ID2 nuclear translocation occurs in $RANK^+$ cells (Kim et al., 2006; Kim et al., 2011), indicating that $K6^+$ BPs in ducts would be a strong candidate of $RANK^+$ cells in pubertal mammary gland development. Thus, side branch formation might require both progesterone-sensing PGR^+ luminal cells and adjacent $K6^+$ BPs in ducts.

$K6^+$ BPs reside in TEBs and leave their progeny on ducts during ductal elongation (Grimm et al., 2006), and nuclear translocation of ID2 in remaining $K6^+$ BPs on primary ducts may induce side branching. Intriguingly, primary ducts and TEBs have $K6^+$ cells and $K8^+$ luminal cells (Smith et al., 1990; Sun et al., 2010) but few $CD61^+$ LPs, indicating that there is a $CD61^+$ LP-independent luminal differentiation pathway in TEBs. $K6^+$ BPs in TEBs appear to differentiate into mature luminal cells through $CD61^-$ LPs, whereas $K6^+$ BPs remaining in the middle of ducts differentiate into $CD61^+$ LPs by progesterone-mediated nuclear translocation of ID2 to form side branches. This can explain why *Id2*$^{-/-}$ mice showed severe defects in side branching but exhibited normal TEBs despite having few $CD61^+$ LPs. Collectively, my findings suggest that nuclear ID2 induces side branching by promoting the differentiation of $K6^+$ BPs into $CD61^+$ LPs at putative

side branching points, and that a $CD61^+$ LP-independent luminal differentiation pathway could be involved in the primary ductal elongation.

Signal transducer and activator of transcription 5 (STAT5) is a well-known master regulator of alveologenesis and induces the differentiation of $CD61^+$ LPs during pregnancy (Cui et al., 2004; Miyoshi et al., 2001; Vafaizadeh et al., 2010). Even in nulliparous mice, loss of STAT5 results in impaired differentiation of $CD61^+$ LPs with side branching defects (Santos et al., 2010; Yamaji et al., 2009), indicating phenocopy between *Id2*$^{-/-}$ and *Stat5*$^{-/-}$ mice. Meanwhile, RANKL is a pivotal downstream mediator of progesterone in side branching and luminal differentiation (Beleut et al., 2010; Fernandez-Valdivia et al., 2009; Grimm et al., 2016; Lee et al., 2013; Mukherjee et al., 2010; Obr et al., 2013; Rajaram et al., 2015) and translocates ID2 into the nucleus (Kim et al., 2006; Kim et al., 2011). Obr et al. reported that STAT5 induces the transcription of *Rankl* by cooperating with progesterone (Obr et al., 2013), suggesting that STAT5 may induce side branching and luminal lineage differentiation through the RANKL-ID2 pathway. Collectively, ID2 may be a downstream mediator of the progesterone/STAT5 signaling in luminal lineage differentiation and side branch formation.

To elucidate how ID2 drives the differentiation of $K6^+$ BPs into $CD61^+$ LPs, I conducted RNA-sequencing with mRNA from WT, *Id2*$^{-/-}$ and *NLS-Id2* Tg MECs, and examined expression patterns of several factors/mediators which are related in luminal lineage differentiation, such as *Gata-3, Elf-5* (Asselin-Labat et

al., 2007; Chakrabarti et al., 2012; Choi et al., 2009; Kouros-Mehr et al., 2008; Kouros-Mehr et al., 2006; Lee et al., 2013; Oakes et al., 2008), *Stat5* (Miyoshi et al., 2001; Santos et al., 2008, 2010; Watson and Burdon, 1996; Yamaji et al., 2009), and *Notch* (Bouras et al., 2008; Lafkas et al., 2013; Raafat et al., 2011; Sale et al., 2013). However, I could not find any difference of these genes between WT, *Id2*$^{-/-}$ and *NLS-Id2* Tg MECs (data not shown), suggesting that ID2 may drives luminal lineage commitment through independent mechanism to already-known luminal lineage differentiating factors/mediators. With deep analysis of RNA-seq data, I found significant induction of CDK inhibitor gene expressions, consistent with K6^{+} BP data in Figure 26 and 27. Collectively, ID2 might induce luminal lineage differentiation through noble pathway.

In this study, I established a new tissue preparation method that enables the observation of ductal trees of mammary glands easily, and found that most CD61^{+} LPs reside in budding and side branches but not in TEBs or primary ducts. Based on my results, I suggest that CD61 is a marker for side branches in young virgin mice. My study provided important insights into the differentiation of progenitors in ductal morphogenesis of mammary glands *in vivo*. Further studies identifying ID2 binding partners and the related molecular mechanisms will help us to understand luminal lineage commitment in developing mammary glands.

Figure 42. Schematic view for defects on *Id2*$^{-/-}$ mice. (A) After puberty, young virgin *Id2*$^{-/-}$ mice showed severe side branching defects with increased and decreased numbers of K6^{+} BPs and CD61^{+} LPs, respectively. **(B)** In putative side branching points, nuclear ID2 would induce differentiation of K6^{+} BPs into CD61^{+} LPs to form new side branches.

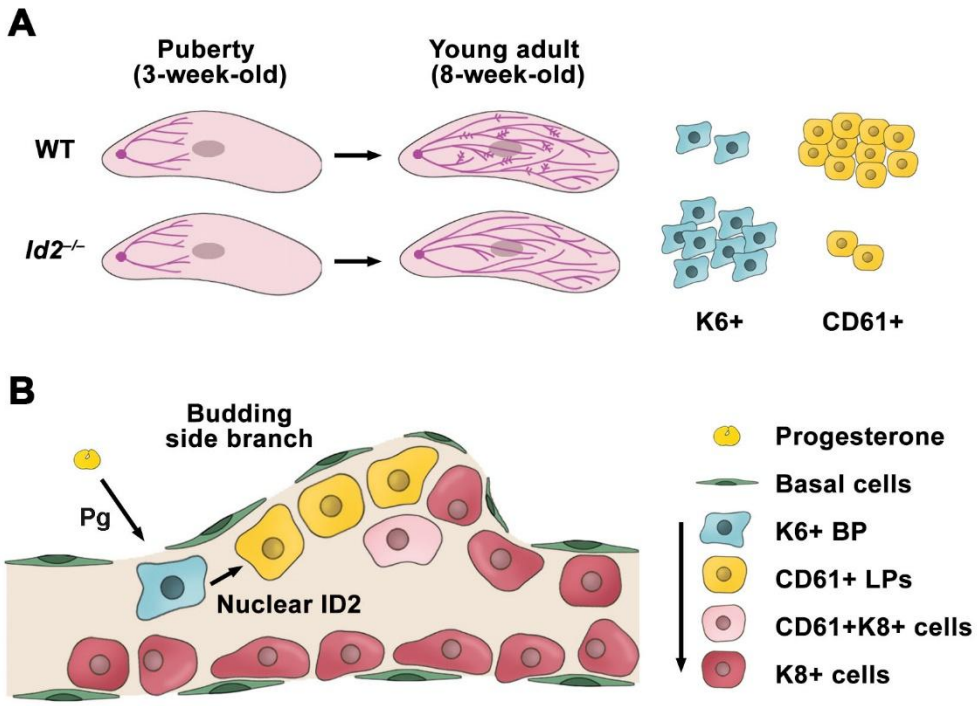
A
Puberty
(3-week-old)
Young adult
(8-week-old)
WT
Id2−/−
K6+
CD61+
B
Budding
side branch
Pg
Nuclear ID2
Progesterone
Basal cells
K6+ BP
CD61+ LPs
CD61+K8+ cells
K8+ cells

MATERIALS & METHODS

Mice

All animal experiments were conducted using 8-week-old virgin female mice on a FVB/N background, unless otherwise noted (for example, 12-week-old lactation day 1 [L1] or 20-week-old mice). All 'N' in my manuscript means the number of mice. The estrus cycle of mice was checked daily at noon, and only mice in diestrus were chosen for experiments. Generation of *Id2*$^{-/-}$ mice was described previously (Yokota et al., 1999), and mice were a kind gift from Dr. Yokota (Department of Molecular Genetics, Graduate School of Medicine, Kyoto University, Japan). *Hemagglutinin* and *nuclear localized sequence* tagged *Id2* transgenic (*MMTV-HA-NLS-Id2 Tg*) mice were generated as previously characterized method (Kim et al., 2011). Briefly, to construct the vector, HA-tagged murine *NLS-Id2* cDNA was ligated into the *MMTV* long terminal repeat (LTR) plasmid (*pMMTV-NLS-Id2*), which was microinjected into the pronuclei of fertilized one-cell zygotes from FVB/N mice. All mice were maintained at the animal facilities of Seoul National University. All animal experiments were approved by Seoul National University Institutional Animal Care and Use Committee and performed in accordance with the guidelines of the institution.

Vaginal staining

For vaginal staining, phosphate-buffered saline (PBS)-immersed cotton swabs

were inserted into the vagina (once a day, at noon). The vaginal secretion was placed on slide glass, dried, stained with hematoxylin for 30 s, briefly rinsed with 1' distilled water (DW), and then examined using a fluorescent microscope (Axio Imager A2; Zeiss) equipped with a SPOT Flex camera. All mice were sacrificed at diestrus.

Mammary epithelial cell (MEC) preparation and single-cell dissociation

Because large numbers of adipocytes can disrupt the accuracy of experimental results from MECs, I skimmed off the fat from MECs using single-cell dissociation according to the protocol described by STEMCELL Technologies. Briefly, dissected inguinal fat pads were chopped into small pieces and incubated in dissociation medium containing Epicult-B medium (cat. no. 05611 and 05612; STEMCELL Technologies) with 10× collagenase/hyaluronidase (cat. no. 07912; STEMCELL Technologies), 5% fetal bovine serum (FBS; cat. no. SH30070.03; Thermo), 10 ng/mL epidermal growth factor (EGF; cat. no. PMG8043; Invitrogen, Carlsbad, CA, USA), 10 ng/mL basic fibroblast growth factor (bFGF; cat. no. F0291; Sigma, St. Louis, MO, USA), 10 ng/mL cholera toxin (cat. no. C8052; Sigma), and 0.0004% heparin (cat. no. 07980; STEMCELL Technologies) on a 360° rotator at 37°C for 4 or 6 h for flow cytometry or RNA/protein extraction, respectively. The suspension was then centrifuged, and the supernatant (mostly adipocytes) was discarded. The pellet was resuspended in red blood cell (RBC) lysis buffer (150 mM NH_4Cl and 10 mM Tris-HCl) and HF solution (Hanks'

Balanced Salt Solution plus 2% FBS) at a 4:1 ratio, gently inverted for 5 min at room temperature, and centrifuged at 350 × *g* for 5 min. The supernatant was then discarded. Pellets were resuspended with 0.25% trypsin-ethylenediaminetetraacetic acid (EDTA; cat. no. 15400; Gibco) and mixed well by pipetting for 3 min. Next, a 10:1 ratio of 5 mg/mL dispase (cat. no. 07913; STEMCELL Technologies) and DNase1 (cat. no. 07900; STEMCELL Technologies) for 1 min sequentially (with HF neutralizing and centrifugation after each step). The neutralized solution of MECs was passed through a 40-μm cell strainer (cat. no. 93040; SPL) before centrifugation. Adipocyte-free single MECs were used for subsequent experiments (compared with control groups, mRNA expression of adipocyte markers was decreased 7.2–10.7-fold after dissociation for 6 h; data not shown).

Flow cytometry

After 4 h of incubation and single-cell dissociation, 1×10^6 MECs were stained for 30 min on ice with the 100ng of following primary antibodies: anti-CD24-PE/Cy7 (cat. no. 101821; BioLegend), anti-CD29-APC (cat. no. 102215; BioLegend), anti-CD61-FITC (cat. no. 104305; BioLegend), anti-CD49b-PE (cat. no. 103506; BioLegend), biotinylated anti-CD31 (cat. no. 102404; BioLegend), biotinylated anti-CD45 (cat. no. 103104; BioLegend), biotinylated anti-CD140b (cat. no. 136010; BioLegend), and biotinylated anti-Ter119 (cat. no. 116204; BioLegend). To sort out endothelial cells and leukocytes, MECs were incubated on ice with streptavidin-PerCP (cat. no. 405213; Biolegend) for 15 min. To sort out dead cells,

7-aminoactinomycin D (7-AAD; cat. no. SML1633; Sigma) was added (1:1000) to fluorescence-activated cell sorting (FACS) buffer (PBS plus 2% FBS) and incubated for 15 min just before use. Flow cytometry was conducted using FACS Calibur, Canto and Aria3 instruments (BD). I used at least 20,000 cells for CD29-CD24 gating. Data were analyzed by FlowJo software.

RNA extraction, reverse transcription polymerase chain reaction (RT-PCR), and quantitative PCR (qPCR)

After 6 h of incubation and single-cell dissociation, RNA was extracted from MECs using an RNeasy Mini kit (cat. no. 74104; Qiagen, Valencia, CA, USA). Resulting RNAs were reverse transcribed, and qRT-PCR was conducted. qRT-PCR primer sequence information is given below.

– *Uxt*: 5'-CTGGAACTGACACTGGCTGA-3'

5'- GATGCAGTCAATGGGGAGAT -3'

– *β-Actin*: 5'- TGTTACCAACTGGGACGACA -3'

5'- GGGGTGTTGAAGGTCTCAAA -3'

– *Gapdh*: 5'- AACTTTGGCATTGTGGAAGG -3'

5'- ACACATTGGGGGTAGGAACA -3'

– *18s rRNA*: 5'- CGCGGTTCTATTTTGTTGGT -3'

5'- AGTCGGCATCGTTTATGGTC -3'

– *Id2*: 5'- ATCAGCCATTTCACCAGGAG -3'

5'- TCCCCATGGTGGGAATAGTA -3'

– *K8*: 5’- ATCGAGATCACCACCTACCG -3’

5’- TGAAGCCAGGGCTAGTGAGT -3’

– *K18*: 5’-AAGGTCTGGAAGCCCAGATT-3’

5’-CTTGGTGGTGACAACTGTGG-3’

– *K19*: 5’-ACCCTCCCGAGATTACAACC-3’

5’-CAAGGCGTGTTCTGTCTCAA-3’

– *Sma*: 5’-CTGACAGAGGCACCACTGAA-3’

5’-CATCTCCAGAGTCCAGCACA-3’

– *K14*: 5’-AGATGTGACCTCCACCAACC-3’

5’-AGGGACAATACAGGGGCTCT-3’

– *Cd61*: 5’-GCTCATTGGCCTTGCTACTC-3’

5’-CCCGGTAGGTGATATTGGTG-3’

– *K6a*: 5’-ATGAGCAGCTCCCTGTGAGT-3’

5’-TACGAGGAAGCCAAGAGCAT-3’

– *p15*: 5’-GGCAAGTGGAGACGGTG-3’

5’-GTTGGGTTCTGCTCCGTG-3’

– *p16*: 5’-CTTCTCACCTCGCTTGTCAC-3’

5’-CGAACTTCACCAAGAAAACC-3’

– *p21*: 5’-CTTGCACTCTGGTGTCTGAG-3’

5’-GCACTTCAGGGTTTTCTCTTG-3’

– *p27*: 5’-AAGGGCCAACAGAACAGAAG-3’

5’-GGATGTCCATTCAATGGAGT-3’

– *β-casein*: 5’-AAGCTAAAGCCACCATCCTT-3’

5’-CAGCTGGGTCTGAGAAGAAA-3’

– *Wap*: 5’-TGAGGGCACAGAGTGTATCA-3’

5’-TCGCTGGAGCATTCTATCTT-3’

– *α-lactalbumin*: 5’-TGAATGGGCCTGTGTTTTAT-3’

5’-CACGCTATGTCATCATCCAA-3’

– *Neu*: 5’-CCCATCAGAGTGATGTGTGG-3’

5’-GGGCGACATTCAGAGTCAAT -3’

– *c-Jun*: 5’-TCCCCTATCGACATGGAGTC-3’

5’-TTTTGCGCTTTCAAGGTTTT-3’

– *c-Myc*: 5’-TGAAGGCTGGATTTCCTTTG-3’

5’-TTCTCTTCCTCGTCGCAGAT-3’

– *Trp53*: 5’-AGAGACCGCCGTACAGAAGA-3’

5’-CTGTAGCATGGGCATCCTTT-3’

– *Stat3*: 5’-ACCCAACAGCCGCCGTAG-3’

5’-CAGACTGGTTGTTTCCATTC-3’

Among the four housekeeping genes (*Uxt*, *β-actin*, *Gapdh*, and *18s rRNA*) used in this study, *Uxt* (ubiquitously expressed transcript) has been reported to be the most stable housekeeping gene for normalizing mRNA levels in bovine mammary tissues (Bionaz and Loor, 2007). Because *Uxt* showed great stability

under various conditions, such as age, biological condition (virgin or pregnancy), and experimental condition (short and long dissociation time), I used *Uxt* results for normalization of relative mRNA expression as a representative if other housekeeping genes showed similar patterns.

Protein isolation and western blotting

For protein isolation, MECs were dissociated for 6 h and lysed using RIPA buffer (cat. no. 89900; Thermo Scientific) and a Sonic 130-Watt Ultrasonic Processor (BioExpress). For western blotting, proteins were transferred to polyvinylidene difluoride (PVDF) membranes, and membranes were then blocked with TBS-T (1× TBS plus 0.1% Triton X-100) containing 5% skim milk (cat. no. 232100; BD) at room temperature for 1 h. To detect specific proteins of interest, the following antibodies were used: anti-β-tubulin (cat. no. ab15568; Abcam, 1:2000), anti-β-actin (cat. no. A2066; Sigma, 1:1000), anti-E-cadherin (cat. no. 610182; BD, 1:1000), anti-K8 (cat. no. Troma-1; Developmental Studies Hybridoma Banks, 1:2500), anti-K6 (cat. no. PRB-169P; Covance, 1:1000), anti-SMA (cat. no. ab7817; Abcam, 1:2000), anti-CD61 (cat. no. 13166; Cell Signaling Technology, Danvers, MA, USA, 1:1000). Horseradish peroxidase (HRP)-conjugated secondary antibodies were then used. Luminescence was detected with a FUSION Solo instrument (Vilber Lourmat).

Carmine-alum (C-A) staining

For C-A staining, freshly dissected inguinal fat pads were flattened and stretched on slide glass as much as possible. To remove fat from mammary glands, I placed fat pads in Clarke's solution (75% EtOH plus 25% acetic anhydride) for 16–18 h at room temperature. After brief washing with 70% EtOH, fat pads were stained in C-A solution (0.2% carmine, 0.5% aluminum potassium sulfate, and 0.02% thymol) for 16–18 h. Destaining was conducted using 2% HCl plus 70% EtOH for 4–6 h. Tissues were then incubated with increasing concentrations of EtOH (70%, 95%, and 100%) for dehydration and cleared using xylene. Samples were stored in methyl salicylate. The results were obtained using a Nikon SMZ18 microscope equipped with a Nikon DS-Ri2 camera.

Histological analysis

For histological analysis, inguinal fat pads were fixed with 4% paraformaldehyde overnight at 4°C (no longer than 24 h) and washed in 1' DW for 1 day. After EtOH-xylene-paraffin dehydration processing, the tissues were embedded in paraffin and sliced to 5-μm thickness. For immunohistochemistry, rehydrated mammary gland tissues were boiled at 95°C for 20 min with antigen-retrieval buffer (10 mM Tris plus 1 mM EDTA, pH 9.0) to expose antigenic epitopes. The tissues were incubated with blocking buffer (10% goat serum, 5% bovine serum albumin [BSA], 0.3% Triton X-100 in PBS) for 2–4 h in a humidified chamber at room temperature and then incubated overnight at 4°C with the following primary antibodies: anti-K8 (cat. no. Troma-1; Developmental Studies Hybridoma Banks, 1:1000), anti-K6 (cat.

no. PRB-169P; Covance, 1:1000), anti-SMA (cat. no. ab7817; Abcam, 1:500), anti-CD61 (cat. no. 13166; Cell Signaling Technology, Danvers, MA, USA, 1:500), anti-p27 (cat. no. sc-1641; Santa Cruz, 1:200), anti-HA (cat. no. sc-7392 and sc-805; Santa Cruz, 1:200 each). Fluorescent probes were affixed using Alexa 488, Alexa 594 and Alexa 647-conjugated antibodies (Invitrogen) targeting the primary antibodies (1:300). Hoechst (cat. no. H3570; Invitrogen, 1:1000) was used to detect nuclei, and slides were mounted with Vectashield (cat. no. H-1000; Vector Laboratories, Burlingame, CA, USA). Immunofluorescence was detected using a confocal laser-scanning microscope (LSM700; Carl Zeiss and TCS SP8; Leica). For hematoxylin and eosin (H&E) staining, the tissues were placed in hematoxylin and eosin for 5 min and 15 s, respectively, with washing using 1' DW following each step (brief destaining was followed after hematoxylin staining with 1% HCl). After dehydration (increasing concentrations of EtOH, followed by xylene incubation) and mounting (cat. no. 6769007; Thermo Scientific), tissues were analyzed using a fluorescence microscope (Axio Imager A2; Zeiss) equipped with a SPOT Flex camera.

Flattened tissue preparation

For flattened tissue preparation, freshly dissected inguinal fat pads were washed in PBS briefly and sandwiched between two pieces of 3MM paper (with stretching of the tissues as far as possible). Staple the tissues on 3MM paper firmly not to detach from 3MM paper. The subsequent procedures were the same as described above.

Because of horizontal attachment of mammary gland tissues on 3MM paper, tissues were shrunk only vertically and still had the same horizontal attachment area after undergoing EtOH-xylene-paraffin dehydration. Since not all ducts and side branches elongated in parallel to the cutting plane, it is difficult to find intact branching structures in cross section with traditional tissue preparation methods. However, this compression enabled detection of more branches per cross-sectional area and yielded a relatively intact side branch structure.

BrdU incorporation assay

Three hours before sacrifice, mice were intraperitoneally injected with BrdU (50 μg/g body weight; cat. no. B5002; Sigma). For immunofluorescence, I used anti-BrdU (cat. no. ab92837; Abcam) as a primary antibody. Secondary antibodies were the same as described in the Histological analysis section.

Whole tissue clearing and 3D imaging

For 3D imaging, I performed CUBIC (Clear, Unobstructed Brain Imaging Cocktails and computational analysis) method as previously reported (Lloyd-Lewis et al., 2016; Susaki et al., 2014) with minor modification. Briefly, mammary fat pads were fixed with 4% paraformaldehyde overnight at 4°C and 1hr at RT, and washed with PBS (1 hr x 2 times). The tissues were incubated in Reagent 1 (25% (w/w) urea, 25% (w/w) N,N,N',N'-tetrakis(2-hydroxypropyl)ethylenediamine, 15% (w/w) triton x-100 in distilled water) for 3 days at 37°C, and washed with PBS (1hr)

and 0.1% PBST (1hr x 2 times) at RT. The tissues were incubated with blocking buffer (10% goat serum in 0.5% PBST) overnight at 4°C, and then incubated for 4 days at 4°C with gentle rocking and the following primary antibodies: anti-K8 (cat. no. Troma-1; Developmental Studies Hybridoma Banks, 1:1000), anti-CD61 (cat. no. 13166; Cell Signaling Technology, Danvers, MA, USA, 1:500). Fluorescent probes were affixed using Alexa 488 and Alexa 594-conjugated antibodies (Invitrogen) targeting the primary antibodies (1:300) for 2 days at 4°C with gentle rocking, and Hoechst (cat. no. H3570; Invitrogen, 1:1000) was used to detect nuclei. PBST (0.3%) wash was followed after each antibody and Hoechst incubation (1hr x 3 times). The tissues were incubated in Reagent 2 (44% (w/w) sucrose, 22% (w/w) urea, 9% (w/w) 2,2',2''-nitrilotriethanol, 0.1% (w/w) triton x-100 in distilled water) for tissue clearing at least 4 days at 37°C with gentle rocking. K8 was detected easily after 1-2 days clearing, but CD61 begin to be detected after 4 days clearing. Immunofluorescence was detected using a confocal laser-scanning microscope (TCS SP8; Leica). Movies (supplementary movie1, 2) were comprised of 1000 frame of pictures (60 frames per second)

Cell lines and immunocytochemistry (ICC)

For ICC, I used the HC11 cell line which I purchased in ATCC. After clearance for Mycoplasma contamination, HC11 cells were incubated with RPMI 1640 medium (cat. no. SH30027.01; Hyclone) containing 10% FBS, 10 ng/mL EGF, 100× glutamax (cat. no. 35050; Gibco), 5 μg/mL insulin (cat. no. 91077C-100MG;

Sigma), and 100× Antibiotic-Antimycotic (cat. no. 15240; Gibco) at 37°C in an incubator containing 5% CO_2. For vector transfection, I used *pcDNA-HA- Id2*, and *NLS-Id2* vectors. I mixed vectors (2 μg, each) and 8 μg polyethylenimine (PEI; cat. no. 23966-2; Polyscience) with 200 μl pre-warmed Opti-MEM (cat. no. 11058021; Gibco) and incubated for 10 min at room temperature. For transfection with Metafectene reagent (cat. no. T020-1.0; Biontex), I mixed vectors (3 μg, each) and 9 μg Metafectene with 100 μl pre-warmed Opti-MEM and incubated for 10 min at room temperature. This mixture was then added to HC11 cells in 6-well plates with none-RPMI 1640 medium and incubated for 4–6 h at 37°C in an incubator containing 5% CO_2. The medium was replaced with complete RPMI 1640 medium, and the cells were incubated for more 2 days. For $CD61^{-}CD49b^{-}$ single cell sorting, mammary epithelial cells in inguinal fat pads were dissociated and stained with antibodies, as described 'Flow cytometry' section. Flow cytometry was conducted using FACS AriaⅢ instruments (BD), and sorted single cells were spun down on slide glasses using Cytospin4 (Thermo scientific). For ICC, cells were fixed for 30 min on ice with 4% PFA and permeabilized for 30 min at room temperature with 0.2% Triton X-100 in PBS (PBST). After brief washing with 0.1% PBST, the cells were incubated with blocking buffer (2% bovine serum albumin [BSA] in 0.1% PBST) for 30 min and then incubated overnight at 4°C with the following primary antibodies: anti-CD61 (cat. no. sc-365679; Santa Cruz, 1:500), anti-K6 (cat. no. PRB-169P; Covance, 1:1000), anti-HA (cat. no. sc-7392 and sc-805; Santa Cruz, 1:200 each). Fluorescent probes were affixed using Alexa 488-conjugated and

Alexa 594-conjugated antibodies (Invitrogen) against primary antibodies (1:300). Hoechst (cat. no. H3570; Invitrogen, 1:1000) was used to detect nuclei, and slides were mounted with Vectashield (cat. no. H-1000; Vector Laboratories). Immunofluorescence was detected using a confocal laser-scanning microscope (TCS SP8; Leica).

Transplantation

Inguinal fat pads from 8-week-old WT and *Id2*$^{-/-}$ mice were dissected and minced in chopping buffer (dissociation medium without collagenase/hyaluronidase and cholera toxin). A small part of minced inguinal fat pads (approximately 1 mm^3) from WT and *Id2*$^{-/-}$ mice was transplanted into the left and right cleared fat pad of a 3 week-old virgin *WT* mice, respectively (Grimm et al., 2006; Naylor and Ormandy, 2002; Welm et al., 2008). To show ductal elongation evidently, I implanted MECs at the edge of cleared fat pads of recipients. After 8–10 weeks, ductal outgrowth was compared each other in a mouse by C-A staining.

Ovariectomy and hormone administration

For observation of outgrowth of side branches, 5-week-old mice were anesthetized by intraperitoneal injection of 2,2,2-tribromoethanol (Avertin; cat. no. T48402-25G; 250 μg/g; Sigma) and ovariectomized. Since side branches were evident in 6-week-old WT virgin mice, I used 5-week-old mice in order to not confuse newly formed side branches induced by ID2 from natural side branching induced by endogenous

hormones. After a 3-week recovery period (Ingberg et al., 2012), a 2-cm silastic tube (cat. no. 508-009; Dow Corning) with 17β-estradiol (cat. no. E8875-1G; Sigma) and progesterone (cat. no. P0130-25G; Sigma), with both ends blocked using 3-mm wooden caps, were implanted; 17β-estradiol and progesterone were dissolved in corn oil (cat. no. C8267-500ML; Sigma) at concentrations of 30 μg/mL and 1 mg/mL, respectively, based on references (Aupperlee et al., 2013; Joshi et al., 2010; Strom et al., 2012). After an additional 1 week for hormone administration, mammary glands were used for C-A staining. For flow cytometry and analysis of luminal lineage differentiation, 3-week-old mice were ovariectomized to minimize the effects of endogenous ovarian hormones on luminal lineage differentiation. After a 3-week recovery period, silastic tubes with hormones were implanted. After 3-week hormone administration, mammary glands were used for flow cytometry to examine luminal lineage differentiation.

Statistical analysis

All statistical analyses were performed using GraphPad Prism 5 (GraghPadSoftware) and Excel 2016 (Microsoft). All of the error bars represent the standard error of the mean (SEM). Data were analyzed using the two-way ANOVA analysis and the two-sample *t*-test (for a difference in mean). The two-way ANOVA analysis was performed in Figure 34A and 36C. The two sample *t*-test was performed in all graph data. A *p*-value of <0.05 was considered statistically significant at the 95% confidence level. The number of biological (non-technical)

replicates for each experiment is indicated in the figure legends. All representative images shown are from experiments that have been performed at least in triplicate.

Data availability.

Source data of represented figures and all other data supporting my findings are available from the corresponding author on request.

REFERENCES

Asselin-Labat, M.L., Sutherland, K.D., Barker, H., Thomas, R., Shackleton, M., Forrest, N.C., Hartley, L., Robb, L., Grosveld, F.G., van der Wees, J., *et al.* (2007). Gata-3 is an essential regulator of mammary-gland morphogenesis and luminal-cell differentiation. Nat Cell Biol *9*, 201-209.

Atwood, C.S., Hovey, R.C., Glover, J.P., Chepko, G., Ginsburg, E., Robison, W.G., and Vonderhaar, B.K. (2000). Progesterone induces side-branching of the ductal epithelium in the mammary glands of peripubertal mice. J Endocrinol *167*, 39-52.

Aupperlee, M.D., Leipprandt, J.R., Bennett, J.M., Schwartz, R.C., and Haslam, S.Z. (2013). Amphiregulin mediates progesterone-induced mammary ductal development during puberty. Breast Cancer Res *15*, R44.

Beleut, M., Rajaram, R.D., Caikovski, M., Ayyanan, A., Germano, D., Choi, Y., Schneider, P., and Brisken, C. (2010). Two distinct mechanisms underlie progesterone-induced proliferation in the mammary gland. Proc Natl Acad Sci U S A *107*, 2989-2994.

Benezra, R. (2001). The Id proteins: targets for inhibiting tumor cells and their blood supply. Biochim Biophys Acta *1551*, F39-47.

Best, S.A., Hutt, K.J., Fu, N.Y., Vaillant, F., Liew, S.H., Hartley, L., Scott, C.L., Lindeman, G.J., and Visvader, J.E. (2014). Dual roles for Id4 in the regulation of estrogen signaling in the mammary gland and ovary. Development *141*, 3159-3164.

Bionaz, M., and Loor, J.J. (2007). Identification of reference genes for quantitative

real-time PCR in the bovine mammary gland during the lactation cycle. Physiol Genomics *29*, 312-319.

Bouras, T., Pal, B., Vaillant, F., Harburg, G., Asselin-Labat, M.L., Oakes, S.R., Lindeman, G.J., and Visvader, J.E. (2008). Notch signaling regulates mammary stem cell function and luminal cell-fate commitment. Cell Stem Cell *3*, 429-441.

Brisken, C. (2013). Progesterone signalling in breast cancer: a neglected hormone coming into the limelight. Nat Rev Cancer *13*, 385-396.

Brisken, C., and Duss, S. (2007). Stem Cells and the Stem Cell Niche in the Breast: An Integrated Hormonal and Developmental Perspective. Stem Cell Reviews *3*, 147-156.

Brisken, C., Heineman, A., Chavarria, T., Elenbaas, B., Tan, J., Dey, S.K., McMahon, J.A., McMahon, A.P., and Weinberg, R.A. (2000). Essential function of Wnt-4 in mammary gland development downstream of progesterone signaling. Genes Dev *14*, 650-654.

Bu, W., Chen, J., Morrison, G.D., Huang, S., Creighton, C.J., Huang, J., Chamness, G.C., Hilsenbeck, S.G., Roop, D.R., Leavitt, A.D.*, et al.* (2011). Keratin 6a marks mammary bipotential progenitor cells that can give rise to a unique tumor model resembling human normal-like breast cancer. Oncogene *30*, 4399-4409.

Byers, S.L., Wiles, M.V., Dunn, S.L., and Taft, R.A. (2012). Mouse estrous cycle identification tool and images. PLoS One *7*, e35538.

Chakrabarti, R., Wei, Y., Romano, R.A., DeCoste, C., Kang, Y., and Sinha, S. (2012). Elf5 regulates mammary gland stem/progenitor cell fate by influencing

notch signaling. Stem Cells *30*, 1496-1508.

Choi, Y.S., Chakrabarti, R., Escamilla-Hernandez, R., and Sinha, S. (2009). Elf5 conditional knockout mice reveal its role as a master regulator in mammary alveolar development: failure of Stat5 activation and functional differentiation in the absence of Elf5. Dev Biol *329*, 227-241.

Ciarloni, L., Mallepell, S., and Brisken, C. (2007). Amphiregulin is an essential mediator of estrogen receptor alpha function in mammary gland development. Proc Natl Acad Sci U S A *104*, 5455-5460.

Coppe, J.P., Smith, A.P., and Desprez, P.Y. (2003). Id proteins in epithelial cells. Exp Cell Res *285*, 131-145.

Cui, Y., Riedlinger, G., Miyoshi, K., Tang, W., Li, C., Deng, C.X., Robinson, G.W., and Hennighausen, L. (2004). Inactivation of Stat5 in mouse mammary epithelium during pregnancy reveals distinct functions in cell proliferation, survival, and differentiation. Mol Cell Biol *24*, 8037-8047.

Davis, F.M., Lloyd-Lewis, B., Harris, O.B., Kozar, S., Winton, D.J., Muresan, L., and Watson, C.J. (2016). Single-cell lineage tracing in the mammary gland reveals stochastic clonal dispersion of stem/progenitor cell progeny. Nat Commun *7*, 13053.

de Candia, P., Benera, R., and Solit, D.B. (2004). A role for Id proteins in mammary gland physiology and tumorigenesis. Adv Cancer Res *92*, 81-94.

Desgrosellier, J.S., Lesperance, J., Seguin, L., Gozo, M., Kato, S., Franovic, A., Yebra, M., Shattil, S.J., and Cheresh, D.A. (2014). Integrin alphavbeta3 drives slug activation and stemness in the pregnant and neoplastic mammary gland. Dev Cell

30, 295-308.

Dong, J., Huang, S., Caikovski, M., Ji, S., McGrath, A., Custorio, M.G., Creighton, C.J., Maliakkal, P., Bogoslovskaia, E., Du, Z.*, et al.* (2011). ID4 regulates mammary gland development by suppressing p38MAPK activity. Development *138*, 5247-5256.

Fata, J.E., Kong, Y.Y., Li, J., Sasaki, T., Irie-Sasaki, J., Moorehead, R.A., Elliott, R., Scully, S., Voura, E.B., Lacey, D.L.*, et al.* (2000). The osteoclast differentiation factor osteoprotegerin-ligand is essential for mammary gland development. Cell *103*, 41-50.

Fernandez-Valdivia, R., Mukherjee, A., Ying, Y., Li, J., Paquet, M., DeMayo, F.J., and Lydon, J.P. (2009). The RANKL signaling axis is sufficient to elicit ductal side-branching and alveologenesis in the mammary gland of the virgin mouse. Dev Biol *328*, 127-139.

Fu, N.Y., Rios, A.C., Pal, B., Law, C.W., Jamieson, P., Liu, R., Vaillant, F., Jackling, F., Liu, K.H., Smyth, G.K.*, et al.* (2017). Identification of quiescent and spatially restricted mammary stem cells that are hormone responsive. Nat Cell Biol *19*, 164-176.

Gajewska, M., Zielniok, K., and Motyl, T. (2013). Autophagy in Development and Remodelling of Mammary Gland.

Gjorevski, N., and Nelson, C.M. (2011). Integrated morphodynamic signalling of the mammary gland. Nat Rev Mol Cell Biol *12*, 581-593.

Grimm, S.L., Bu, W., Longley, M.A., Roop, D.R., Li, Y., and Rosen, J.M. (2006).

Keratin 6 is not essential for mammary gland development. Breast Cancer Res *8*, R29.

Grimm, S.L., Hartig, S.M., and Edwards, D.P. (2016). Progesterone Receptor Signaling Mechanisms. J Mol Biol.

Hannezo, E., Scheele, C., Moad, M., Drogo, N., Heer, R., Sampogna, R.V., van Rheenen, J., and Simons, B.D. (2017). A Unifying Theory of Branching Morphogenesis. Cell *171*, 242-255 e227.

Haslam, S.Z. (1988a). Acquisition of estrogen-dependent progesterone receptors by normal mouse mammary gland. Ontogeny of mammary progesterone receptors. J Steroid Biochem *31*, 9-13.

Haslam, S.Z. (1988b). Progesterone effects on deoxyribonucleic acid synthesis in normal mouse mammary glands. Endocrinology *122*, 464-470.

Hennighausen, L., and Robinson, G.W. (2005). Information networks in the mammary gland. Nat Rev Mol Cell Biol *6*, 715-725.

Howlin, J., McBryan, J., and Martin, F. (2006). Pubertal mammary gland development: insights from mouse models. J Mammary Gland Biol Neoplasia *11*, 283-297.

Ingberg, E., Theodorsson, A., Theodorsson, E., and Strom, J.O. (2012). Methods for long-term 17beta-estradiol administration to mice. Gen Comp Endocrinol *175*, 188-193.

Joshi, P.A., Jackson, H.W., Beristain, A.G., Di Grappa, M.A., Mote, P.A., Clarke, C.L., Stingl, J., Waterhouse, P.D., and Khokha, R. (2010). Progesterone induces

adult mammary stem cell expansion. Nature *465*, 803-807.

Junankar, S., Baker, L.A., Roden, D.L., Nair, R., Elsworth, B., Gallego-Ortega, D., Lacaze, P., Cazet, A., Nikolic, I., Teo, W.S.*, et al.* (2015). ID4 controls mammary stem cells and marks breast cancers with a stem cell-like phenotype. Nat Commun *6*, 6548.

Kim, N.S., Kim, H.J., Koo, B.K., Kwon, M.C., Kim, Y.W., Cho, Y., Yokota, Y., Penninger, J.M., and Kong, Y.Y. (2006). Receptor activator of NF-kappaB ligand regulates the proliferation of mammary epithelial cells via Id2. Mol Cell Biol *26*, 1002-1013.

Kim, N.S., Kim, H.T., Kwon, M.C., Choi, S.W., Kim, Y.Y., Yoon, K.J., Koo, B.K., Kong, M.P., Shin, J., Cho, Y.*, et al.* (2011). Survival and differentiation of mammary epithelial cells in mammary gland development require nuclear retention of Id2 due to RANK signaling. Mol Cell Biol *31*, 4775-4788.

Kouros-Mehr, H., Kim, J.W., Bechis, S.K., and Werb, Z. (2008). GATA-3 and the regulation of the mammary luminal cell fate. Curr Opin Cell Biol *20*, 164-170.

Kouros-Mehr, H., Slorach, E.M., Sternlicht, M.D., and Werb, Z. (2006). GATA-3 maintains the differentiation of the luminal cell fate in the mammary gland. Cell *127*, 1041-1055.

Lafkas, D., Rodilla, V., Huyghe, M., Mourao, L., Kiaris, H., and Fre, S. (2013). Notch3 marks clonogenic mammary luminal progenitor cells in vivo. J Cell Biol *203*, 47-56.

Lasorella, A., Benezra, R., and Iavarone, A. (2014). The ID proteins: master

regulators of cancer stem cells and tumour aggressiveness. Nat Rev Cancer *14*, 77-91.

Lasorella, A., Uo, T., and Iavarone, A. (2001). Id proteins at the cross-road of development and cancer. Oncogene *20*, 8326-8333.

Lee, H.J., Gallego-Ortega, D., Ledger, A., Schramek, D., Joshi, P., Szwarc, M.M., Cho, C., Lydon, J.P., Khokha, R., Penninger, J.M.*, et al.* (2013). Progesterone drives mammary secretory differentiation via RankL-mediated induction of Elf5 in luminal progenitor cells. Development *140*, 1397-1401.

Lloyd-Lewis, B., Davis, F.M., Harris, O.B., Hitchcock, J.R., Lourenco, F.C., Pasche, M., and Watson, C.J. (2016). Imaging the mammary gland and mammary tumours in 3D: optical tissue clearing and immunofluorescence methods. Breast Cancer Res *18*, 127.

Lo, P.K., Kanojia, D., Liu, X., Singh, U.P., Berger, F.G., Wang, Q., and Chen, H. (2012). CD49f and CD61 identify Her2/neu-induced mammary tumor-initiating cells that are potentially derived from luminal progenitors and maintained by the integrin-TGFbeta signaling. Oncogene *31*, 2614-2626.

Lyden, D., Young, A.Z., Zagzag, D., Yan, W., Gerald, W., O'Reilly, R., Bader, B.L., Hynes, R.O., Zhuang, Y., Manova, K.*, et al.* (1999). Id1 and Id3 are required for neurogenesis, angiogenesis and vascularization of tumour xenografts. Nature *401*, 670-677.

Lydon, J.P., DeMayo, F.J., Funk, C.R., Mani, S.K., Hughes, A.R., Montgomery, C.A., Jr., Shyamala, G., Conneely, O.M., and O'Malley, B.W. (1995). Mice lacking

progesterone receptor exhibit pleiotropic reproductive abnormalities. Genes Dev *9*, 2266-2278.

Miyoshi, K., Meyer, B., Gruss, P., Cui, Y., Renou, J.P., Morgan, F.V., Smith, G.H., Reichenstein, M., Shani, M., Hennighausen, L.*, et al.* (2002). Mammary epithelial cells are not able to undergo pregnancy-dependent differentiation in the absence of the helix-loop-helix inhibitor Id2. Mol Endocrinol *16*, 2892-2901.

Miyoshi, K., Shillingford, J.M., Smith, G.H., Grimm, S.L., Wagner, K.U., Oka, T., Rosen, J.M., Robinson, G.W., and Hennighausen, L. (2001). Signal transducer and activator of transcription (Stat) 5 controls the proliferation and differentiation of mammary alveolar epithelium. J Cell Biol *155*, 531-542.

Mori, S., Inoshima, K., Shima, Y., Schmidt, E.V., and Yokota, Y. (2003). Forced expression of cyclin D1 does not compensate for Id2 deficiency in the mammary gland. FEBS Letters *551*, 123-127.

Mori, S., Nishikawa, S.I., and Yokota, Y. (2000). Lactation defect in mice lacking the helix-loop-helix inhibitor Id2. EMBO J *19*, 5772-5781.

Mukherjee, A., Soyal, S.M., Li, J., Ying, Y., He, B., DeMayo, F.J., and Lydon, J.P. (2010). Targeting RANKL to a specific subset of murine mammary epithelial cells induces ordered branching morphogenesis and alveologenesis in the absence of progesterone receptor expression. FASEB J *24*, 4408-4419.

Naylor, M.J., and Ormandy, C.J. (2002). Mouse strain-specific patterns of mammary epithelial ductal side branching are elicited by stromal factors. Dev Dyn *225*, 100-105.

Niola, F., Zhao, X., Singh, D., Castano, A., Sullivan, R., Lauria, M., Nam, H.S., Zhuang, Y., Benezra, R., Di Bernardo, D., *et al.* (2012). Id proteins synchronize stemness and anchorage to the niche of neural stem cells. Nat Cell Biol *14*, 477-487.

Norton, J.D., Deed, R.W., Craggs, G., and Sablitzky, F. (1998). Id helix-loop-helix proteins in cell growth and differentiation. Trends Cell Biol *8*, 58-65.

Oakes, S.R., Naylor, M.J., Asselin-Labat, M.L., Blazek, K.D., Gardiner-Garden, M., Hilton, H.N., Kazlauskas, M., Pritchard, M.A., Chodosh, L.A., Pfeffer, P.L., *et al.* (2008). The Ets transcription factor Elf5 specifies mammary alveolar cell fate. Genes Dev *22*, 581-586.

Obr, A.E., Grimm, S.L., Bishop, K.A., Pike, J.W., Lydon, J.P., and Edwards, D.P. (2013). Progesterone receptor and Stat5 signaling cross talk through RANKL in mammary epithelial cells. Mol Endocrinol *27*, 1808-1824.

Park, M.J., Park, S.H., Moon, S.E., Koo, J.S., Moon, H.S., and Joo, B.S. (2013). Decreased Expression of Inhibitor of DNA-binding (Id) Proteins and Vascular Endothelial Growth Factor and Increased Apoptosis in Ovarian Aging. Dev Reprod *17*, 17-24.

Parrinello, S., Lin, C.Q., Murata, K., Itahana, Y., Singh, J., Krtolica, A., Campisi, J., and Desprez, P.Y. (2001). Id-1, ITF-2, and Id-2 comprise a network of helix-loop-helix proteins that regulate mammary epithelial cell proliferation, differentiation, and apoptosis. J Biol Chem *276*, 39213-39219.

Prat, A., and Perou, C.M. (2009). Mammary development meets cancer genomics.

Nat Med *15*, 842-844.

Prater, M.D., Petit, V., Alasdair Russell, I., Giraddi, R.R., Shehata, M., Menon, S., Schulte, R., Kalajzic, I., Rath, N., Olson, M.F*., et al.* (2014). Mammary stem cells have myoepithelial cell properties. Nat Cell Biol *16*, 942-950, 941-947.

Raafat, A., Goldhar, A.S., Klauzinska, M., Xu, K., Amirjazil, I., McCurdy, D., Lashin, K., Salomon, D., Vonderhaar, B.K., Egan, S*., et al.* (2011). Expression of Notch receptors, ligands, and target genes during development of the mouse mammary gland. J Cell Physiol *226*, 1940-1952.

Rajaram, R.D., Buric, D., Caikovski, M., Ayyanan, A., Rougemont, J., Shan, J., Vainio, S.J., Yalcin-Ozuysal, O., and Brisken, C. (2015). Progesterone and Wnt4 control mammary stem cells via myoepithelial crosstalk. EMBO J *34*, 641-652.

Rios, A.C., Fu, N.Y., Lindeman, G.J., and Visvader, J.E. (2014). In situ identification of bipotent stem cells in the mammary gland. Nature *506*, 322-327.

Robinson, G.W. (2007). Cooperation of signalling pathways in embryonic mammary gland development. Nat Rev Genet *8*, 963-972.

Ruzinova, M.B., and Benezra, R. (2003). Id proteins in development, cell cycle and cancer. Trends Cell Biol *13*, 410-418.

Sale, S., Lafkas, D., and Artavanis-Tsakonas, S. (2013). Notch2 genetic fate mapping reveals two previously unrecognized mammary epithelial lineages. Nat Cell Biol *15*, 451-460.

Santos, S.J., Haslam, S.Z., and Conrad, S.E. (2008). Estrogen and progesterone are critical regulators of Stat5a expression in the mouse mammary gland.

Endocrinology *149*, 329-338.

Santos, S.J., Haslam, S.Z., and Conrad, S.E. (2010). Signal transducer and activator of transcription 5a mediates mammary ductal branching and proliferation in the nulliparous mouse. Endocrinology *151*, 2876-2885.

Scheele, C.L., Hannezo, E., Muraro, M.J., Zomer, A., Langedijk, N.S., van Oudenaarden, A., Simons, B.D., and van Rheenen, J. (2017). Identity and dynamics of mammary stem cells during branching morphogenesis. Nature.

Shackleton, M., Vaillant, F., Simpson, K.J., Stingl, J., Smyth, G.K., Asselin-Labat, M.L., Wu, L., Lindeman, G.J., and Visvader, J.E. (2006). Generation of a functional mammary gland from a single stem cell. Nature *439*, 84-88.

Shehata, M., Teschendorff, A., Sharp, G., Novcic, N., Russell, I.A., Avril, S., Prater, M., Eirew, P., Caldas, C., Watson, C.J.*, et al.* (2012). Phenotypic and functional characterisation of the luminal cell hierarchy of the mammary gland. Breast Cancer Res *14*, R134.

Smalley, M., and Ashworth, A. (2003). Stem cells and breast cancer: A field in transit. Nat Rev Cancer *3*, 832-844.

Smith, G.H., Mehrel, T., and Roop, D.R. (1990). Differential keratin gene expression in developing, differentiating, preneoplastic, and neoplastic mouse mammary epithelium. Cell Growth Differ *1*, 161-170.

Soyal, S., Ismail, P.M., Li, J., Mulac-Jericevic, B., Conneely, O.M., and Lydon, J.P. (2002). Progesterone's role in mammary gland development and tumorigenesis as disclosed by experimental mouse genetics. Breast Cancer Res *4*, 191-196.

Sternlicht, M.D., Kouros-Mehr, H., Lu, P., and Werb, Z. (2006). Hormonal and local control of mammary branching morphogenesis. Differentiation *74*, 365-381.

Stingl, J. (2009). Detection and analysis of mammary gland stem cells. J Pathol *217*, 229-241.

Stingl, J., Eirew, P., Ricketson, I., Shackleton, M., Vaillant, F., Choi, D., Li, H.I., and Eaves, C.J. (2006). Purification and unique properties of mammary epithelial stem cells. Nature *439*, 993-997.

Strom, J.O., Theodorsson, A., Ingberg, E., Isaksson, I.M., and Theodorsson, E. (2012). Ovariectomy and 17beta-estradiol replacement in rats and mice: a visual demonstration. J Vis Exp, e4013.

Sun, P., Yuan, Y., Li, A., Li, B., and Dai, X. (2010). Cytokeratin expression during mouse embryonic and early postnatal mammary gland development. Histochem Cell Biol *133*, 213-221.

Susaki, E.A., Tainaka, K., Perrin, D., Kishino, F., Tawara, T., Watanabe, T.M., Yokoyama, C., Onoe, H., Eguchi, M., Yamaguchi, S.*, et al.* (2014). Whole-brain imaging with single-cell resolution using chemical cocktails and computational analysis. Cell *157*, 726-739.

Vafaizadeh, V., Klemmt, P., Brendel, C., Weber, K., Doebele, C., Britt, K., Grez, M., Fehse, B., Desrivieres, S., and Groner, B. (2010). Mammary epithelial reconstitution with gene-modified stem cells assigns roles to Stat5 in luminal alveolar cell fate decisions, differentiation, involution, and mammary tumor formation. Stem Cells *28*, 928-938.

Vaillant, F., Asselin-Labat, M.L., Shackleton, M., Forrest, N.C., Lindeman, G.J., and Visvader, J.E. (2008). The mammary progenitor marker CD61/beta3 integrin identifies cancer stem cells in mouse models of mammary tumorigenesis. Cancer Res *68*, 7711-7717.

Van Keymeulen, A., Rocha, A.S., Ousset, M., Beck, B., Bouvencourt, G., Rock, J., Sharma, N., Dekoninck, S., and Blanpain, C. (2011). Distinct stem cells contribute to mammary gland development and maintenance. Nature *479*, 189-193.

Verykokakis, M., Krishnamoorthy, V., Iavarone, A., Lasorella, A., Sigvardsson, M., and Kee, B.L. (2013). Essential functions for ID proteins at multiple checkpoints in invariant NKT cell development. J Immunol *191*, 5973-5983.

Visvader, J.E. (2009). Keeping abreast of the mammary epithelial hierarchy and breast tumorigenesis. Genes Dev *23*, 2563-2577.

Visvader, J.E., and Stingl, J. (2014). Mammary stem cells and the differentiation hierarchy: current status and perspectives. Genes Dev *28*, 1143-1158.

Watson, C.J., and Burdon, T.G. (1996). Prolactin signal transduction mechanisms in the mammary gland: the role of the Jak/Stat pathway. Rev Reprod *1*, 1-5.

Welm, B.E., Dijkgraaf, G.J., Bledau, A.S., Welm, A.L., and Werb, Z. (2008). Lentiviral transduction of mammary stem cells for analysis of gene function during development and cancer. Cell Stem Cell *2*, 90-102.

Woodward, W.A., Chen, M.S., Behbod, F., and Rosen, J.M. (2005). On mammary stem cells. J Cell Sci *118*, 3585-3594.

Yamaji, D., Na, R., Feuermann, Y., Pechhold, S., Chen, W., Robinson, G.W., and

Hennighausen, L. (2009). Development of mammary luminal progenitor cells is controlled by the transcription factor STAT5A. Genes Dev *23*, 2382-2387.

Yokota, Y., Mansouri, A., Mori, S., Sugawara, S., Adachi, S., Nishikawa, S., and Gruss, P. (1999). Development of peripheral lymphoid organs and natural killer cells depends on the helix-loop-helix inhibitor Id2. Nature *397*, 702-706.

Yokota, Y., Mori, S., Narumi, O., and Kitajima, K. (2001). In vivo function of a differentiation inhibitor, Id2. IUBMB Life *51*, 207-214.

Zebedee, Z., and Hara, E. (2001). Id proteins in cell cycle control and cellular senescence. Oncogene *20*, 8317-8325.

국문 초록

ID2 단백질의 유선내강전구세포 분화 유도를 통한 유선 곁가지 생성

유선은 주 가지 (primary duct) 신장 및 곁가지 (side branch) 생성을 통해 유선 조직의 표면적을 최대로 넓힌다. 주 가지는 유두로부터 직접 뻗어 나온 가지이며, 가지의 최전방에 분열이 매우 활발한 세포 덩어리인 말단 싹 (TEB, terminal end bud) 이라는 구조를 가진다. 말단 싹의 분열을 통해 하나였던 주 가지가 둘로 나뉘어지는 방식으로 점차 가지를 늘려가며 유방의 지방조직을 채운다. 이렇게 주 가지의 신장이 일어남과 동시에, 말단 싹 분열과는 독립적인 메커니즘으로 새로운 가지가 주 가지의 가운데 부분으로부터 뻗어 나온다. 이를 측면 가지 형성 혹은 곁가지 형성이라 부른다. 최근의 한 연구팀은 주 가지의 신장 방향 및 신장 속도가 주 가지들 서로간의 공간적 방해를 통해 일어나는 것이라는 예측을 수학적 모델링을 이용해 보고한 바 있다. 하지만 곁가지가 어떠한 방식으로 생성되고 신장되는지에 대한 연구는 아직까지도 보고된 바가 매우 적다.

유선줄기세포 (MaSC, mammary stem cell) 는 이분화전구세포 (bipotent progenitor cell) 로 분화하며, 다시 내강세포 (luminal cell) 혹은 근상피세포 (myoepithelial cell) 계열로 분화할 것이라 추측된다. 하지만 아직까지 유선줄기세포를 특이적으로 표지 할 수 있는 마커가

밝혀지지 않았기 때문에 현재 기술로써는 유선줄기세포가 어떠한 계열의 세포로 분화하는지 또 어떠한 방식으로 분화하는지를 파악하기 매우 힘들며, 실제로도 유선줄기세포 및 이분화전구세포의 특정 계열 분화에 대한 연구가 매우 미흡하다. 따라서 유선줄기세포와 이분화전구세포가 어떠한 메커니즘으로 특정 계열로의 분화를 결정하는지를 밝히는 것은 유선발달 연구에 있어서 매우 중요한 부분이다.

본 연구에서는 ID2 단백질이 $K6^+$ 이분화전구세포를 $CD61^+$ 내강전구세포 (luminal progenitor cell) 로 분화 시키며, 이를 통해 곁가지가 생성될 수 있다는 내용을 새로이 보고하고자 한다. ID2 유전자 결손 쥐는 곁가지 생성 발달이 제대로 일어나지 않으며, $K6^+$ 이분화전구세포가 $CD61^+$ 내강전구세포로 분화하지 않는다. 반대로, ID2 과발현 쥐는 곁가지의 수가 매우 증가하였으며, $K6^+$ 이분화전구세포 역시 $CD61^+$ 내강전구세포로 활발히 분화하였다. 특히, $CD61^+$ 내강전구세포는 주 가지가 아닌 곁가지에서만 특이적으로 발견되는데, 이는 $CD61^+$ 내강전구세포가 곁가지 형성에 영향을 줄 수 있다는 것을 뜻한다. 호르몬 발생을 최소화 시킨 난소절제쥐 (Ovariectomized mice) 연구를 통해, ID2 단백질은 프로게스테론 (progesterone) 의 하위 매개체로써 내강세포계열로의 분화 및 곁가지 생성을 유도한다는 것을 밝혔다.

결론적으로, 본 연구는 ID2 단백질이 프로게스테론 신호의 주된 인자로써, $K6^+$ 이분화전구세포의 $CD61^+$ 내강전구세포로의 분화를 유도함으로써 곁가지를 생성을 일으킨다는 것을 보고하고자 한다.

Key word: 유선, inhibitor of DNA-binding 2 (ID2) 단백질, CD61 유선내강전구세포, 곁가지 생성

Student Number: 2010-23112